DESIGN AND IMPLEMENTATION OF AN EFFICIENT IMAGE COMPRESSOR FOR WIRELESS CAPSULE ENDOSCOPY

A Thesis Submitted to the College of

Graduate Studies and Research

In Partial Fulfillment of the Requirements

For the Degree of Master of Science

In the Department of Electrical and Computer Engineering

University of Saskatchewan

Saskatoon

By

ATAHAR KAMAL MOSTAFA

PERMISSION TO USE

In presenting this thesis in partial fulfilment of the requirements for a Postgraduate degree from the University of Saskatchewan, I agree that the Libraries of this University may make it freely available for inspection. I further agree that permission for copying of this thesis in any manner, in whole or in part, for scholarly purposes may be granted by the professor or professors who supervised my thesis work or, in their absence, by the Head of the Department or the Dean of the College in which my thesis work was done. It is understood that any copying or publication or use of this thesis or parts thereof for financial gain shall not be allowed without my written permission. It is also understood that due recognition shall be given to me and to the University of Saskatchewan in any scholarly use which may be made of any material in my thesis.

Requests for permission to copy or to make other use of material in this thesis in whole or part should be addressed to:

Head of the Department of Electrical and Computer Engineering

57 Campus Drive

University of Saskatchewan

Saskatoon SK S7N 5A9

Canada

ABSTRACT

Capsule endoscope (CE) is a diagnosis tool for gastrointestinal (GI) diseases. Area and power are the two important parameters for the components used in CE. To optimize these two parameters, an efficient image compressor is desired. The mage compressor should be able to sufficiently compress the captured images to save transmission power, retain reconstruction quality for accurate diagnosis and consumes small physical area. To meet all of the above mentioned conditions, we have studied several transform coding based lossy compression algorithms in this thesis.

The core computation tool of these compressors is the Discrete Cosine Transform (DCT) kernel. The DCT accumulates the distributed energy of an image in a small centralized area and supports more compression with non-significant quality degradation. The conventional DCT requires complex floating point multiplication, which is not feasible for wireless capsule endoscopy (WCE) application because of its high implementation cost. So, an integer version of the DCT, known as iDCT, is used in this work. Several low complexity iDCTs along with different color space converters (such as, YUV, YEF, YCgCo) were combined to obtain the desired compression level.

At the end a quantization stage is used in the proposed algorithm to achieve further compression. We have analyzed the endoscopic images and based on their properties, three quantization matrix sets have been proposed for three color planes. The algorithms are verified at both software (using MATLAB) and hardware (using HDL Verilog coding) levels. In the end, the performance of all the proposed schemes has been evaluated for optimal operation in WCE application.

ACKNOWLEDGMENTS

First, I would like to express my gratitude to my supervisors, Dr. Khan A.Wahid and Dr. Seok-Bum Ko for introducing me to this research field and for their continuous support, inspiration, and guidance throughout the project. Their vast knowledge and expertise in this field added considerably to my graduate experience.

Then, I would like to thank my thesis committee for their guidance and insightful comments.

I would also like to acknowledge the financial support from NSERC, Graduate Studies and Research, University of Saskatchewan and Department of Electrical and Computer Engineering, University of Saskatchewan.

Finally, I would like to thank my family for their love, encouragement, and support.

This thesis is dedicated to my loving parents.

TABLE OF CONTENTS

LIST OF TABLES

LIST OF FIGURES

LIST OF ABBREVIATIONS

CE	Capsule Endoscope
CMOS	Complementary-symmetry Metal Oxide Semiconductor
CR	Compression Ratio
CS	Compressed Sensing
DCT	Discrete Cosine Transform
DPCM	Differential Pulse Code Modulation
GI	Gastrointestinal
HVS	Human Visual System
IQI	Image Quality Index
JPEG	Joint Photographic Expert Group
LZ	Lempel-Ziv
MSE	Mean Square Error
NBI	Narrow Band Imaging
PSNR	Peak Signal to Noise Ratio
RF	Radio Frequency
SRAM	Static Random Access Memory
SSIM	Structural Similarity Index
WBI	Wide Band Imaging
WCE	Wireless Capsule Endoscopy

Chapter 1

INTRODUCTION

Digestive tract related diseases, such as, bleeding, ulcer and tumor are quite common and can be cured in their early stages; otherwise they will deteriorate into cancer or other fatal diseases [1]. But it is not easy to diagnose these diseases in their early stage. To detect gastrointestinal (GI) tract diseases, many indirect technologies, such as, angiography, ultrasonography, X radiography (including computer tomography) and scintigraphy have been developed. However, these technologies were reported to have low success rate even for bleeding detection [2, 3], or be rarely helpful unless severely active bleeding [4].

The best way to detect GI diseases is directly viewing the GI tract using endoscopy [5]. After the invention of modern wired endoscopy in 1960's, it became possible to view the entire stomach, the upper small intestine and colon. Endoscopy has become the standard method and the criteria for diagnosing GI diseases in a clinic since it allows clinicians to directly view the GI tract. The functions were widely extended by embedding a biopsy device in the fiber-optic endoscope. Power, video signal and lighting are carried to the digital endoscope using flexible and long cables. A micro camera is assembled on the top end of these cables. The digital wired endoscope is pushed into the GI tract with these cables during the examination course. Lighting source through the fiber-optic bundles lights the GI tract and the micro camera captures images for inspection. These images can be stored and processed with a computer. This kind of wired endoscope is now popular in clinic. Welch Allyn Company, Olympus and Fujinon are successful vendors of digital wired endoscope.

However, the traditional invasive wired endoscopes cannot examine the whole GI tract, leaving the small intestine as a dead zone because of its curvy structure. Moreover, these are inconvenient since the process is painful for patients. Furthermore, the wired endoscopes can perforate the intestine and cross-contamination may occur.

In 2000, wireless capsule endoscopy (WCE) was introduced by Given Imaging Limited [6]. A WCE system consists of four parts: the capsule endoscope (CE), the data receiving box, the working station and the application software as shown in Fig. 1-1 [40]. The typical length and diameter of the CE, is 30 mm and 11 mm respectively, which is small enough to be swallowed by patients [6]. The CE travels through the GI tract with peristalsis and takes images of the GI tract. The images are compressed and transmitted wirelessly to the receiving box which is tied to patient's waist. The CE is powered by cell batteries, which can work continuously up to 8 hours. In 2001, the first clinical trial was carried out [6, 7, 8]. The WCE technology is convenient, safe and a major portion of the GI tract can be examined. Such endoscopy is an effective alternative to traditional wired endoscopy and the state-of-the-art method of diagnosing the GI tract diseases.

Due to the advantages achieved by the CE, it has become an important diagnosis tool in a clinic based on its assets. It has irreplaceable effects especially on the small intestine diagnose, and is mainly used to diagnose bleeding, ulcer, tumors and others. It is the only diagnosis method which could directly view the GI tracts. After Pillcam was introduced by Given Imaging, many types of WCE have been developed, and several commercial WCE products are available in the market. Features of these CEs are summarized in Table 1-1.

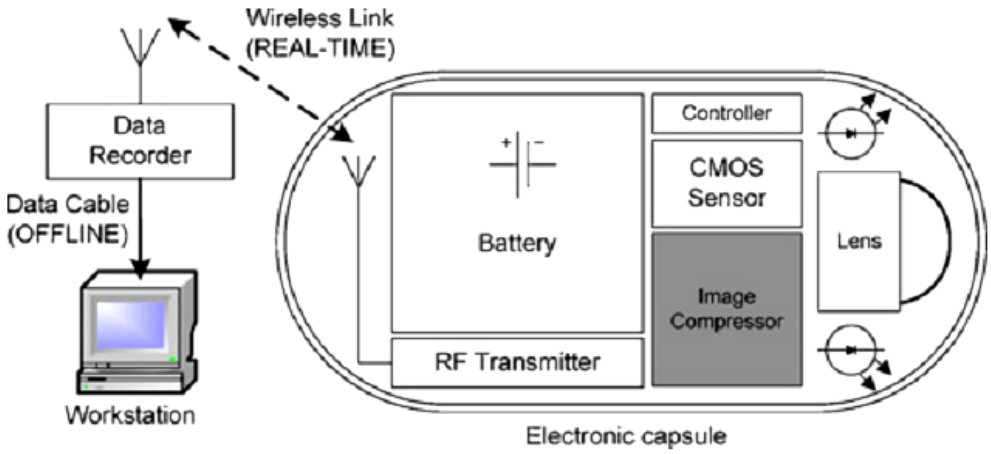

Figure 1-1: A typical WCE system [40]

Table 1-1: Summary of performance of commercially available CEs

Name	**Company**	**Date of release**	**Frame rate (fps)**	**Working time (hours)**
PillCam [6]	Given Imaging	2001	2	6-8
EndoCapsule [9]	Olympus Optical	2005	2	8
OMOM [10][11]	Chongqing Jingshan	2005	2	6~8
MiroCam [12][13]	IntroMedic	2007	3	11

1.1 Related Works

Since the introduction of the first CE, several works have been done in an effort to design an efficient image compressor for the CE. A DCT-based compression is the central idea in most of these works. Other than this approach, Differential Pulse Code Modulation

(DPCM) and Compressed Sensing (CS) based compression schemes were also reported in literature. Wide band endoscopic images are used in most of the works; however narrow band images have been proved more useful in some cases [30].

A low power image compressor for the CE was described in [35]. This was a 2-D DCT based compression scheme which could compress the images by 79.65%. Power saving in this image compressor was achieved by eliminating the color plane converter and demosaicing unit. Thus, it used raw images for the compressor. It proposed low complexity quantization matrices for the three color components. To reduce the memory requirement for the look-up tables and complex computation, Lempel-Ziv (LZ) coding was used for the entropy encoding. This work has a low peak signal-to-noise ratio (PSNR) of 32.51 dB.

In [42], a subsample-based low power compressor was presented for the CE. It isthe extension of [35]. In this work, 82.28 % compression was achieved using subsampling and 2-D DCT. To save the power consumption of demosaicing, raw image was used in this image compressor. A detailed analysis of endoscopic images was presented here. Based on the analysis, blue components were heavily subsampled and passed to the transmitter without any further compression. Green components were lightly subsampled, transformed using the 2-D DCT and quantized before sending to the transmitter. No subsampling was done for the red components since the analysis suggested red components as the most significant component of endoscopic images. For the DCT, 8x8 block size was used for the red components while 4x4 block size was used for green components. This work claimed 98.95% reduction of power consumption when compared to JPEG compression and average PSNR of 40.37 dB for luminance components. LZ77 entropy encoder was used for the entropy encoding. This image compressor has a frame rate of 2 fps (frames per second).

Another DCT based image compressor and detail hardware architecture was presented in [34]. To reduce complex computation of the 2-D DCT, an integer approximation of the DCT was used here. Spectral redundancy of endoscopic images was reduced using YCgCo color plane [18] in this work. Instead of 8 point DCT, 4 point DCT was used for the transformation. Entropy coding for this image compressor was done by two steps. The first one was the Run-Length coding and the second one was Huffman coding. It achieved 10 fps frame rate for 3MHz working frequency, however, compression ratio was only 15% and 25% for the coloscopy and gastroscopy respectively at a PSNR of 36 dB.

A DPCM based image compressor was proposed in [40]. This image compressor worked in YUV color plane to exploit the non-uniform energy distribution of endoscopic images in luminance and chrominance components. To achieve high compression linear subsampling was applied to the chrominance components. An efficient corner clipping algorithm was applied on the captured images to increase the efficiency of the compression process. Subjective evaluation was also done to prove the effectiveness of the compressor. Golomb coding was used for the entropy encoding, which was claimed more suitable for the endoscopic images in YUV plane. This work claimed PSNR of 48 dB at 80% compression ratio; however, it could not transmit more than 2 fps with only 0.042 mW power consumption.

Besides, a CS based image compressor was proposed in [38]. A capsule endoscope prototype was designed in [47] which could capture images in narrow band imaging (NBI) format. Design of a wireless capsule endoscope was described in [36] that worked on JPEG compression engine. In [15], a low power wireless capsule endoscope IC was designed. A DCT based image compressor was presented in [33] for RGB endoscopic images. A wavelet

based image compressor was reported in [37]. An image compressor was proposed in [17], which compressed images using DPCM and worked in a novel YEF color plane.

1.2 Motivation

Now a day, a CE is widely used for diagnosis of GI diseases. But still these commercially available CEs have several limitations. Low frame rate, insufficient working time, low image quality are some of them. From Table 1-1, 3 fps is found as the maximum data rate for the commercially available CEs. But this rate is not sufficient for accurate diagnosis because at low frame rate some interesting zones of GI tract may not available for examination since there is no active motion controller for the CE. A study in [49] showed the completion rate of 71.7% and diagnosis yield of 18.9% for OMOM capsule at 2 fps. Capsule speed is not same in all part of the GI tract. It moves fastest in esophagus, slower in colon and slowest in small intestine. So, some companies designed different types of capsules for different part of the GI tract. Making a CE for all part of the GI tract by increasing the frame rate thus remains as a challenge.

It was reported in [14] that more than 10 hours are required to complete the examination of whole the GI tract. But it is found from the Table 1-1 that except mirocam, none can fulfill this condition. Mirocam could not produce the best results because of its low frame rate. Working time could be increased by adding more batteries to the CE. However, it is not possible due to the area limitation of the CE. So, more research is required to improve the battery run time with increased frame rate.

These limitations of commercially available CEs encourage researchers to design an improved CE. Several designs are reported in literature, some of them were described in the

previous section. But no work could get rid of all these limitations. Some works reported in [15], [39] and [48] can support more than 10-hours runtime, but none of them can transmit images at more than 2 fps. These works also suffered from low reconstruction quality and compression.

All these limitations of the existing CE image compressor worked as motivation for this work. Image compressor and RF transmitter are the two major components and consume most of the power in CE. An efficient image compressor could address both the power consumption and reconstruction image quality issues. So, in this thesis, we have designed an image compressor, which could successfully compress images with minimum power consumption, thus increased working time and frame rate. The efficient algorithm that was used in the image compressors also could recover the compressed image with sufficiently high quality (35dB [31]).

1.3 Thesis Objective

The objective of this thesis is to design an efficient image compressor for the CE which could fulfill two major conditions.

1) Image compressor should use efficient algorithm that can compress the image sufficiently, and at the same time keep the significant information for high quality reconstruction.
2) The image compressor should consume sufficiently low power so that the CE can have more time to possibly examine the whole GI tract at higher frame rate (3 fps).

1.4 Thesis Organization

The thesis consists of six chapters. Chapter 2 presents the overview of an image compressor: classification of image compressors, components of a lossy image compressor and their variety. In Chapter 3, several image compressors have been described. The performance of the compression schemes is evaluated to obtain the most optimal image compressor. Performance evaluation of these designs is presented in Chapter 4. A Description of the hardware and their comparison with other designs are given in Chapter 5. Finally, summary of accomplishment and some future recommendations are presented in Chapter 6.

CHAPTER 2
OVERVIEW OF AN IMAGE COMPRESSOR

Efficient operation of a capsule endoscope (CE) largely depends on the design of an image compressor. It was reported in [15] that 63% of the total power consumed by CE is used for RF data transmission and it could be reduced by 45% by using an efficient image compressor. Image compressor can reduce the image size up to 90% without significant degradation of the reconstructed image quality. When an image is compressed, the number of bits, required to represent the image is reduced and transmission power is decreased to transmit these lower number of bits. This is how an image compressor saves power in a CE. So, designing an efficient image compressor is very important for the power limited wireless capsule endoscopy (WCE) application.

Exploiting the limitations of human visual system (HVS) is the basic technique behind the image compressor. HVS is only sensitive to a limited bandwidth. But conventional image sensors can capture images over a wider bandwidth. Thus a lot of redundancy is added to a color images. Fig. 2-1 shows the sensitivity of human eye at different wavelength [21]. In this figure, human eye sensitivity is represented along y-axis and wavelength is represented along x-axis. It can be seen from Fig. 2-1 that HSV is more sensitive to luminance (represented by V) than chrominance (R, G, B for red, green, blue respectively), so using the same number of bits to represent the luminance and chrominance components adds psycho-visual redundancy. It is also clear from the figure that sensitivity is not same for all the colors, red and green components are more sensitive than the blue components. So, spectral redundancy is introduced in the color images when same number of bits is used to represent all the color components. Other than these two redundancies, spatial

redundancy could exist in an image when there is a little variation between the neighboring pixel values. Image compressors eliminate these redundancies by several methods. Based on how these redundancies are handled, image compressors can be classified into two categories, lossless and lossy compressor. Though lossy compression was used in this thesis to achieve low power consumption by high compression, a brief description of lossless compression has been given here.

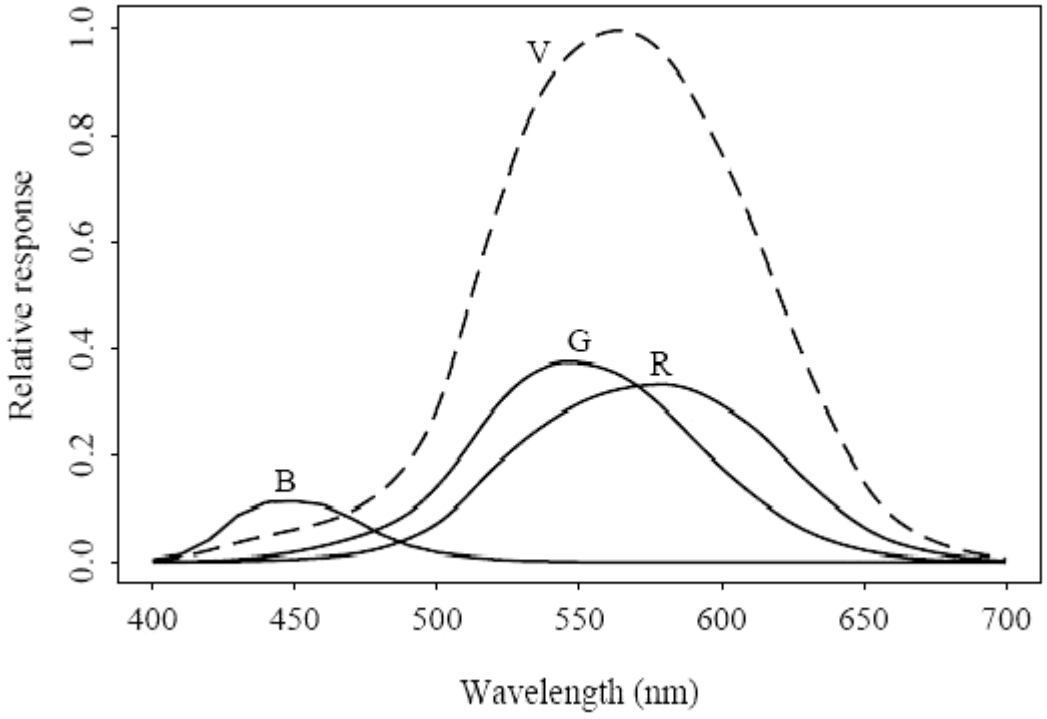

Figure 2-1: Response of eye towards different wavelength [21]

2.1 Lossless Image Compressor

Lossless image compressors use lossless image compression method which only eliminates the spatial redundancies. This compression is done without any data loss. An

image compressed using lossless compression is completely reversible. No distortion is added to the received images except the channel noises. Lossless compression only exploits the spatial redundancy, so compression rate could be very low when the correlation between the neighboring pixels is very low. Image format such as Portable Network Graphics (PNG), Graphic Interchange Format (GIF) is using lossless compression. Compression ratio in this method varies from 20~50%.

Lossless data compression could be classified into two broad categories: fixed length coding and variable length coding.

2.1.1 Fixed Length Coding

Lossless compression could be achieved using fixed length coding, where each symbol is represented using a fixed length code word regardless of their probability. This method works when the symbols are equally probable. But this is not the usual scenario, so fixed length coding is an inefficient way of coding. Binary coding, gray coding, ASCII etc are some example of fixed length coding.

2.1.2 Variable Length Coding

Variable length coding is more efficient than the fixed length coding where each symbol is represented using different number of bits. Assignment of bit to a symbol depends on their probability. Usually most probable symbols are represented using least number of bits. More compression could be achieved using variable length coding. Shannon-Fano

coding, Huffman coding, Arithmetic coding, run-length coding are some examples of variable length coding.

2.2 Lossy Image Compressor

Lossy compressors use more aggressive compression method to achieve high compression ratio. In lossy compression, some redundant information of image is permanently truncated during transmission. This is why some distortion is added to images compressed using this method. Lossy compression exploits all the three redundancies exist in a color image. Joint Photographic Expert Group (JPEG), Progressive Graphic File (PGF) are some image formats using lossy compression. There are several techniques that could be used in lossy image compressors such as color plane converter, chroma subsampling, transform coding and quantization.

2.2.1 Color Plane Converter

Color plane converter is the integral part of the lossy image converter, though it is not compressing an image directly, it separates the chrominance and luminance information of an image. To save bandwidth, chrominance components could be subsampled or quantized. So, color plane converter can be used to get rid of the spectral redundancies.

Blue, red and green are the three components of a digital color images. Thus every color digital image is expressed in RGB (R=red, G=green, B=blue) color plane. The main problem of the RGB plane is the correlation between the color components. So, compressing one component will affect other components. This is why, color plane converter is important for lossy compression. A color plane converter converts an image into one luminance and

two chrominance components. Luminance component holds the structural information while chrominance components hold the color information. Usually, there is not much correlation between the components of a luminance-chrominance color plane. So, chrominance components could be compressed heavily, without affecting the overall reconstruction image quality because structural information is important than the color information for a proper reconstruction. Since components of RGB color plane cannot separate information like this, luminance-chrominance color plane is a better choice for the application where high compression is important.

Several luminance-chrominance based color planes are used in practice. Among them YUV is the most popular. A new color plane YCgCo has a very efficient hardware implementation. A novel YEF color plane was recently proposed specially designed for the WCE application.

2.2.1.1 Color Plane: YUV

YUV color plane has three components. Y is the luminance component and U (blue chrominance) and V (red chrominance) are the chrominance components. YUV color plane was invented when engineers were trying to fit the color signal transmission using the same infrastructure for both black and white and color television. When a color image, captured in RGB format is converted in the YUV plane, its luminance information goes to Y components that gives the grayscale image of that color image and U, V hold the color information. Y component is sufficient for the black and white representation of the color image and all three components produce a color image. So, same transmitter is used to transmit Y,U,V signal. Color television receives all three signals, while black and white television just

ignores the U and V component. Using this method, same infrastructure could be used for both the color and black and white televisions. NTSC and PAL are two analogue television systems who are using YUV format transmission. Digital image compression, such as JPEG and MPEG also use this format.

Several equations are used to convert an RGB image into YUV format. In this thesis we have used the following equation as defined in [22].

$$\begin{bmatrix} Y \\ U \\ V \end{bmatrix} = \frac{1}{8}\left(\begin{bmatrix} 66 & 129 & 25 \\ -38 & -74 & 112 \\ 112 & -94 & -18 \end{bmatrix} \cdot \begin{bmatrix} R \\ G \\ B \end{bmatrix} + \begin{bmatrix} 128 \\ 128 \\ 128 \end{bmatrix} \right) + \begin{bmatrix} 16 \\ 128 \\ 128 \end{bmatrix} \quad \text{..... (2-1) [22]}$$

Where, R,G,B are the red, green and blue components.

To convert the image from YUV to RGB, following equation is used which is also given in [22].

$$\begin{bmatrix} R \\ G \\ B \end{bmatrix} = \frac{1}{8}\left(\begin{bmatrix} 298 & 0 & 409 \\ 298 & -100 & -208 \\ 298 & 516 & 0 \end{bmatrix} \cdot \begin{bmatrix} Y-16 \\ U-128 \\ V-128 \end{bmatrix} + \begin{bmatrix} 128 \\ 128 \\ 128 \end{bmatrix} \right) \quad \text{..... (2-2) [22]}$$

Y, U, V components of an endoscopic image are shown in Fig. 2-2.

Figure 2-2: Different components of an endoscopic image in YUV

2.2.1.2 Color Plane: YCgCo

A new color plane is reported in [18], named YCgCo. This color plane is found in H.264/AVC design. YCgCo is a luminance and chrominance based color plane where Y is the luminance component and Cg, Co are the green and orange chrominance, respectively. This color plane works better than YUV because it can more precisely separate the information of a color image into luminance and chrominance components. So, overall reconstructed image quality will be more insensitive to the compression of chrominance components than YUV color plane. YCgCo also has a simple implementation with compare to YUV. Another advantage of YCgCo is the better coding gain over YUV. It is reported in [18] that the YCoCg leads to a 0.7 dB improvement in coding gain when compared to the several YUV based transforms specified in H.264/AVC Annex E.

Equation (2-3) and (2-4) are used to convert RGB to YCgCo and YCgCo to RGB respectively.

$$\begin{bmatrix} Y \\ Cg \\ Co \end{bmatrix} = \begin{bmatrix} 1/4 & 1/2 & 1/4 \\ -1/4 & 1/2 & -1/4 \\ 1/2 & 0 & -1/2 \end{bmatrix} \begin{bmatrix} R \\ G \\ B \end{bmatrix} \quad \text{..... (2-3) [18]}$$

$$\begin{bmatrix} R \\ G \\ B \end{bmatrix} = \begin{bmatrix} 1 & 1 & -1 \\ 1 & -1 & -1 \\ 1 & 0 & 1 \end{bmatrix} \begin{bmatrix} Y \\ Cg \\ Co \end{bmatrix} \quad \text{..... (2-4) [18]}$$

Y, Cg, Co components of an endoscopic image are shown in Fig. 2-3.

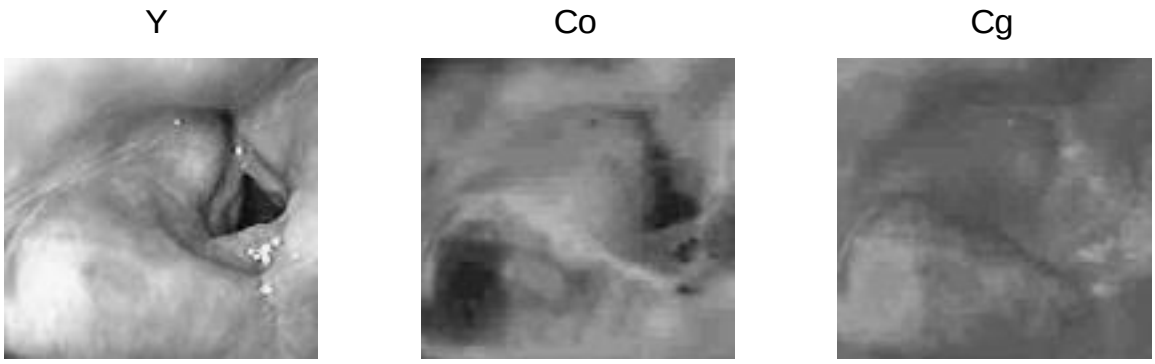

Figure 2-3: Different components of an endoscopic image in YCgCo

2.2.1.3 Color Plane: YEF

In [17], a new color plane was presented named YEF, designed especially for the WCE application. Endoscopic images have dominance in red color, blue and green components are not much significant in endoscopic images. This feature was the motivation of YEF design. YEF has more uncorrelated components when compared to YUV and YCgCo as described in [17]. This color plane is also good in reconstructing endoscopic images. Equation (2-5) is used for converting a pixel from RGB to YEF and (2-6) is used for YEF to RGB conversion. Y, E, F components of an endoscopic image are shown in Fig. 2-4.

$$\begin{bmatrix} Y \\ E \\ F \end{bmatrix} = \begin{bmatrix} 1/4 & 1/2 & 1/4 \\ 1/8 & -1/4 & 1/8 \\ 1/8 & 1/8 & -1/4 \end{bmatrix} \cdot \begin{bmatrix} R \\ G \\ B \end{bmatrix} + \begin{bmatrix} 0 \\ 128 \\ 128 \end{bmatrix} \quad \text{..... (2-5) [17]}$$

$$\begin{bmatrix} R \\ G \\ B \end{bmatrix} = \begin{bmatrix} 1 & 10/3 & 8/3 \\ 1 & -2 & 0 \\ 1 & 2/3 & -8/3 \end{bmatrix} \cdot \begin{bmatrix} Y \\ E-128 \\ F-128 \end{bmatrix} \quad \text{..... (2-6) [17]}$$

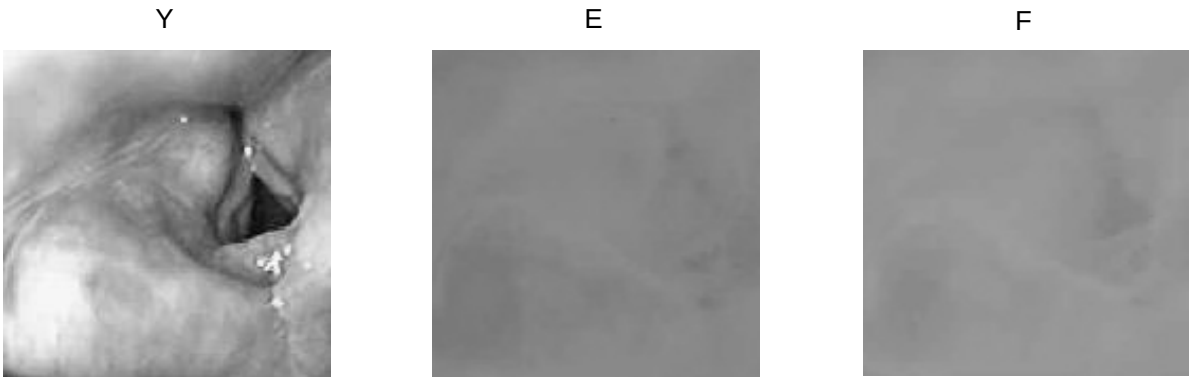

Figure 2-4: Different components of an endoscopic image in YEF

2.2.2 Chroma Subsampling

Chroma subsampling is the technique by which psycho-visual redundancies can be removed from the images. It is known that HSV is less sensitive to color components than the brightness. So, in chroma subsampling, fewer pixels are used to represent the color components of the images than the luminanace components. Several chroma subsampling schemes are available such as 4:4:4, 4:2:2, 4:2:1, 4:1:1, 4:2:0 etc. Other than these, some unconventional subsampling is also possible for some special cases.

In 4:4:4 subsampling scheme, both luminance and chrominance components are sampled with the same rate. So, same bandwidth is used for all the three components. This sampling scheme preserves the spectral redundancy of color image. In 4:2:2 subsampling scheme, luminance component is sampled with double speed of the chrominance components. So, this scheme could save one-third of the bandwidth used for 4:4:4 subsampled images by reducing chrominance component's bit rate. 4:2:2 is more popular compared to other subsampling schemes. Video formats such as AVC-Intra 100, Digital Betacam, DVCPRO50, DVCPRO HD etc are using this subsampling scheme.

The 4:2:1 is a theoretically defined subsampling scheme which has a little practical application. In this subsampling scheme, resolution of one chrominance component is half of the other while luminance component preserve the full resolution. In 4:1:1, total bandwidth demand could be reduced to half by taking one out of four pixels of the chrominance components. It saves half bandwidth as is used by the 4:4:4 subsampling scheme. NTSC, PAL use 4:1:1 subsampling scheme.

4:2:0 is different than the other subsampling scheme. This popular subsampling scheme reduces the vertical resolution for the chrominance as well as the horizontal resolution, which is not done in any other subsampling schemes. Average of the four neighboring pixels for the chrominance component is taken for processing in this scheme. In this format, horizontal resolution is twice the resolution of 4:1:1 but the vertical resolution is reduced by half. Same bandwidth is used for 4:2:0 and 4:1:1. 4:2:0 format could be found in JPEG/JIFF, MJPEG, VC-1 encoders.

Different subsampling schemes are illustrated in Fig. 2-5.

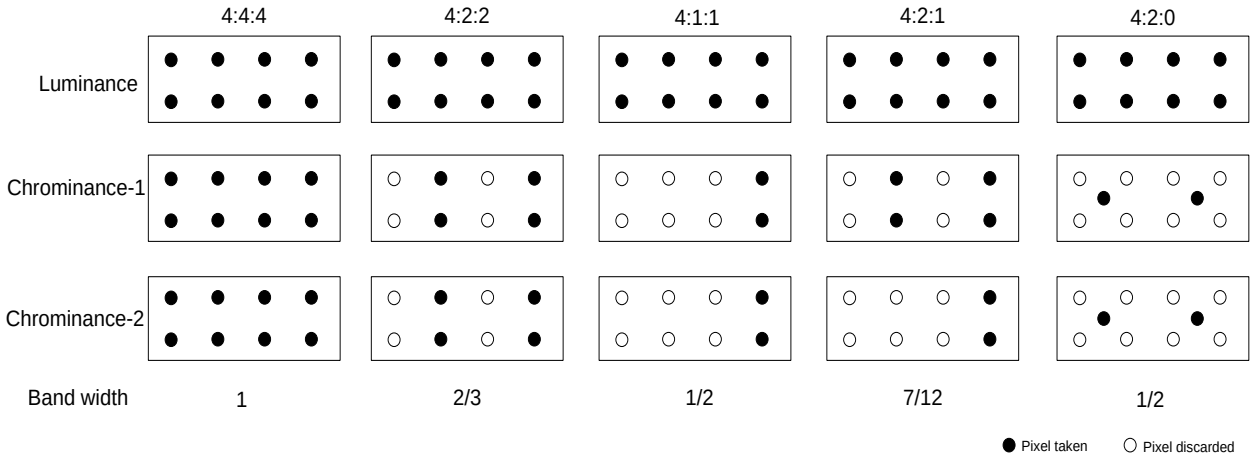

Figure 2-5: Comparison between different subsampling schemes

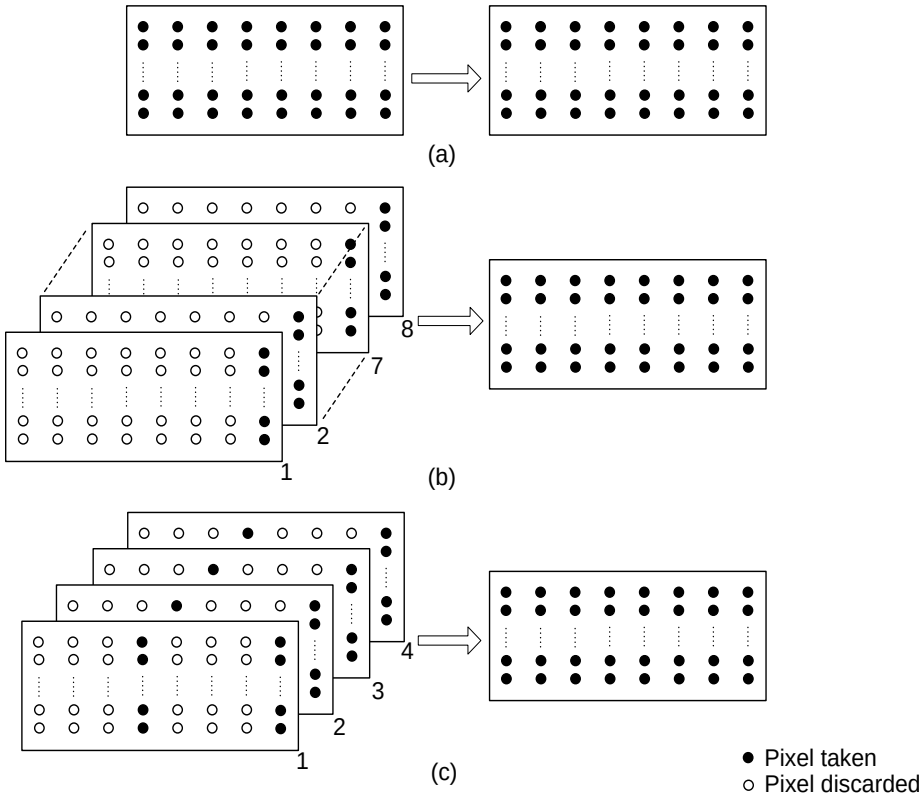

Figure 2-6. (a) Unaffected Luminance component. (b) &(c) Subsampling of chrominance components.

In this thesis, some unconventional subsampling schemes, such as, 8:4:4, 8:2:4, 8:1:4, 8:1:2, 8:2:2, 8:1:1, 16:1:2, 16:1:1 have been applied to the chroma components. All of these were horizontal subsampling. In all cases, luminance component was kept unaffected, only the chroma components were subsampled according to the subsampling scheme. For example, in case of 8:1:2 subsampling, one out of eight columns of 8x8 chrominance-1 blocks were taken for transform coding. Since we have used 8x8 Discrete Cosine Transform (DCT), so eight blocks of chrominance-1 component reduces to one block after subsampling. Finally, this 8x8 block is processed for further compression. Chrominance-2 component is subsampled similarly, except here one out of four columns is taken. There would be a certain

delay of transmission between a luminance block and its corresponding chrominance blocks. However, this delay will not put any adverse effect on the image reconstruction because all the components of a particular frame will be transmitted in the adjacent time. The whole 8:1:2 subsampling process is shown in Fig. 2-6.

Distortion due to the subsampling is obvious, especially when such aggressive subsampling is done. However, little variation of the neighboring pixel values of the chrominance components of an endoscopic image keeps this distortion minimum. Compression of the DCT based transformation lies in the redundancy between adjacent pixels. Here, we have done the DCT by taking pixels those lie in 2 to 16 pixels away from each other. But still good compression can be expected because of the high redundancy of the chrominance components of endoscopic images.

2.2.3 Transform Coding

Transform coding is a very widely used and efficient compression technique. Transform coding changes the spectral information distribution of an image. Usually, significant information of color image is distributed all over the images, so it becomes difficult for the compressor to differentiate between significant and non-significant information. Transform coding can redistribute the information to their corresponding spectrum. So, by filtering, non-significant information can be removed during compression. Several transform coding could be used in the lossy compression technique. All of them use the same transform equation:

$$T(u,v) = \sum_{x=0}^{n-1}\sum_{y=0}^{n-1} g(x,y)\cdot r(x,y,u,v) \quad \text{..... (2-7)}$$

Where, $T(u,v)$ is the transformed coefficients, $g(x,y)$ is the original image components, and $r(x,y,u,v)$ is the basis function for the transformation. Based on this basis function; several transform coding could be achieved.

In image compression, transform coding is usually done by the matrix operation. A 2-D forward image transform could be achieved using the following matrix multiplication:

$$T = X \cdot I \cdot X' \quad \text{..... (2-9)}$$

Where, X is the transform coefficient matrix, I is the image matrix, and T is the transformed image coefficient matrix. This transform coefficient is different for different coding techniques and based on their basis function.

Karhunen Loeve Transform (KLT), Discrete Fourier Transform (DFT), Walsh-Hadamard Transform (WHT), Discrete Cosine Transform (DCT), Discrete Wavelet Transform (DWT) are some well-known transform techniques. Among these transforms, KLT has the best coding efficiency but not possible to implement in practice because coefficients of KLT are random variables.

DCT is the closest approximation of KLT. It can represent an image with a small number of low frequency components. DCT uses block based transformation. Commonly used block sizes are 4x4, 8x8, and 16x16. When the transformation block size is large, more compression could be achieved but reconstructed images suffer from some artifacts. These artifacts can be removed using smaller block size but this reduces the compression ratio. So, 8x8 block size has been chosen in this work to obtain the optimum result. Several versions of DCT are used in image compression. DCT-II is the most common. Other than this several integer DCT (iDCT) and Binary DCT (BinDCT) are also popular for their easy implementation.

2.2.3.1 DCT-II

DCT-II is the most common DCT transform. It is used in JPEG, MJPEG, MPEG compression. DCT-II has a close similarity with Discrete Fourier Transform (DFT). An 8-point 2-D DCT-II can be achieved using (2-10).

$$F_{u,v} = \frac{C(u)C(v)}{4}\sum_{x=0}^{7}\sum_{y=0}^{7} f_{x,y}\cos\left[\frac{(2x+1)u\pi}{16}\right]\cos\left[\frac{(2y+1)v\pi}{16}\right] \text{..... (2-10)}$$

Here, $F_{u,v}$ is transformed coefficient for the time-domain coefficient of $f_{x,y}$ and

$$C(u), C(v) = \begin{cases} 1 & for\ u, v \neq 0 \\ \frac{1}{\sqrt{2}} & for\ u, v = 0 \end{cases}.$$

In image transform, 2-D transform is usually obtained using the matrix multiplication as shown in (2-9). Transform coefficient matrix for the DCT-II is given below.

$$\begin{bmatrix} 0.3536 & 0.3536 & 0.3536 & 0.3536 & 0.3536 & 0.3536 & 0.3536 & 0.3536 \\ 0.4904 & 0.4157 & 0.2778 & 0.0975 & -0.0975 & -0.2778 & -0.4157 & -0.4904 \\ 0.4619 & 0.1913 & -0.1913 & -0.4619 & -0.4619 & -0.1913 & 0.1913 & 0.4619 \\ 0.4157 & -0.0975 & -0.4904 & -0.2778 & 0.2778 & 0.4904 & 0.0975 & -0.4157 \\ 0.3536 & -0.3536 & -0.3536 & 0.3536 & 0.3536 & -0.3536 & -0.3536 & 0.3536 \\ 0.2778 & -0.4904 & 0.0975 & 0.4157 & -0.4157 & -0.0975 & 0.4904 & -0.2778 \\ 0.1913 & -0.4619 & 0.4619 & -0.1913 & -0.1913 & 0.4619 & -0.4619 & 0.1913 \\ 0.0975 & -0.2778 & 0.4157 & -0.4904 & 0.4904 & -0.4157 & 0.2778 & -0.0975 \end{bmatrix}$$

2.2.3.2 iDCT

DCT-II is very popular for image and video compression but its implementation cost is high because of the fraction coefficients. To resolve this problem, DCT with integer coefficients are implemented in several video coding standards. DCT with integer coefficients are called integer DCT or iDCT. Different video coding standards are using

different iDCT transform matrix. In this work, we have experimented with iDCTs defined in H.264, AVS and VC-1.

H.264 is the most popular video coding standard in present time. Its final drafting was completed in May 2003. It supports 4 and 8-point DCTs. Blue-ray disk, HD-DVD use H.264 coding. Equation (2-11) presents the transform matrix presented in H.264 codec. Note that, the integer coefficients in the matrix are pre-defined and cannot be modified.

$$\begin{bmatrix} 8 & 8 & 8 & 8 & 8 & 8 & 8 & 8 \\ 12 & 10 & 6 & 3 & -3 & -6 & -10 & -12 \\ 8 & 4 & -4 & -8 & -8 & -4 & 4 & 8 \\ 10 & -3 & -12 & -6 & 6 & 12 & 3 & -10 \\ 8 & -8 & -8 & 8 & 8 & -8 & -8 & 8 \\ 6 & -12 & 3 & 10 & -10 & -3 & 12 & -6 \\ 4 & -8 & 8 & -4 & -4 & 8 & -8 & 4 \\ 3 & -6 & 10 & -12 & 12 & -10 & 6 & -3 \end{bmatrix} \quad \text{..... (2-11)}$$

VC-1 was developed by Microsoft as a video coding standard for windows media player and released in April, 2006. It is also a DCT-based coding standard supports 4 and 8-point DCT. Windows media player, blue-ray disc support video compression using this standard. The iDCT matrix defined in VC-1 is given in (2-12).

$$\begin{bmatrix} 12 & 12 & 12 & 12 & 12 & 12 & 12 & 12 \\ 16 & 15 & 9 & 4 & -4 & -9 & -15 & -16 \\ 16 & 6 & -6 & -16 & -16 & -6 & 6 & 16 \\ 15 & -4 & -16 & -9 & 9 & 16 & 4 & -15 \\ 12 & -12 & -12 & 12 & 12 & -12 & -12 & 12 \\ 9 & -16 & 4 & 15 & -15 & -4 & 16 & -9 \\ 6 & -16 & 16 & -6 & -6 & 16 & -16 & 6 \\ 4 & -9 & 15 & -16 & 16 & -15 & 9 & -4 \end{bmatrix} \quad \text{..... (2-12)}$$

AVS is a coding standard developed by the People's Republic of China to reduce their dependence on the foreign intellectual properties used in digital media technology. Its

first trial is done in March, 2005. CBHD, China's high-definition video disc format supports AVS. AVS is a DCT based coder uses the iDCT transform matrix of (2-13).

$$\begin{bmatrix} 8 & 8 & 8 & 8 & 8 & 8 & 8 & 8 \\ 10 & 9 & 6 & 2 & -2 & -6 & -9 & -10 \\ 10 & 4 & -4 & -10 & -10 & -4 & 4 & 10 \\ 9 & -2 & -10 & -6 & 6 & 10 & 2 & -9 \\ 8 & -8 & -8 & 8 & 8 & -8 & -8 & 8 \\ 6 & -10 & 2 & 9 & -9 & -2 & 10 & -6 \\ 4 & -10 & 10 & -4 & -4 & 10 & -10 & 4 \\ 2 & -6 & 9 & -10 & 10 & -9 & 6 & -2 \end{bmatrix} \quad \text{..... (2-13)}$$

2.2.3.3 BinDCT

BinDCT is defined in [19] and [20]. This is a multiplier less lifting-scheme based approximation of DCT. Coefficients of the BinDCT transform matrices are easily implementable using the lifting scheme. Even if these are not adopted in any video coding standard, they have shown good promise for JPEG, H.263+ and lossless compression techniques. BinDCT matrices defined in [19] and [20] is given in (2-14) and (2-15) respectively.

$$\begin{bmatrix} 1 & 1 & 1 & 1 & 1 & 1 & 1 & 1 \\ 15/16 & 101/128 & 35/64 & 1/4 & -1/4 & -35/64 & -101/128 & -15/16 \\ 3/4 & 1/2 & -1/2 & -3/4 & -3/4 & -1/2 & 1/2 & 3/4 \\ 1/2 & 2/32 & -11/16 & -1/2 & 1/2 & 11/16 & -3/32 & -1/2 \\ 1/2 & -1/2 & -1/2 & 1/2 & 1/2 & -1/2 & -1/2 & 1/2 \\ 1 & -23/16 & -1/8 & 1 & -1 & 1/8 & 23/16 & -1 \\ 1/2 & -1 & 1 & -1/2 & -1/2 & 1 & -1 & 1/2 \\ 1/4 & -21/32 & 13/16 & -1 & 1 & -13/16 & 21/32 & -1/4 \end{bmatrix} \quad \text{..... (2-14)}$$

$$\begin{bmatrix} 1/2 & 1/2 & 1/2 & 1/2 & 1/2 & 1/2 & 1/2 & 1/2 \\ 1/2 & 1/2 & 3/16 & 0 & 0 & -3/16 & -1/2 & -1/2 \\ 55/128 & 3/16 & -3/16 & -55/128 & -55/128 & -3/16 & 3/16 & 55/128 \\ 9/32 & -1/8 & -19/64 & -1/4 & 1/4 & 19/64 & 1/8 & -9/32 \\ 1/4 & -1/4 & -1/4 & 1/4 & 1/4 & -1/4 & -1/4 & 1/4 \\ 7/16 & -3/4 & 7/32 & 1/2 & -1/2 & -7/32 & 3/4 & -7/16 \\ -3/16 & 1/2 & -1/2 & 3/16 & 3/16 & -1/2 & 1/2 & -3/16 \\ -1/16 & 1/4 & -13/32 & 1/2 & -1/2 & 13/32 & -1/4 & 1/16 \end{bmatrix} \quad \text{..... (2-15)}$$

2.2.4 Quantization

In quantization stage, redundant image components are truncated. It is commonly known that HSV is not equally sensitive to all frequency components. In [16], it was reported that HSV sensitivity is high to low spatial frequency (also called radial frequency, expressed in terms of cycles/degree) zone, which represents the general information about the shape, and exponentially decreases in the high spatial frequency zone, which represents the abrupt spatial change. High compression could be achieved by discarding the high frequency components without adding significant distortion to the reconstructed image. Actually, quantization unit works as a compliment of the transform unit. In transform unit, distributed energy is accumulated in different frequency components, and then high frequency components are discarded by dividing them with a large number since these components are not that important. A typical quantization matrix is shown in Table 2-1.

Operation of a quantization unit is illustrated in Fig. 2-7. Here A_1 is the image block after transformation and Q_1 is the quantization matrix. Usually, the transform coefficient

block and the quantization matrix are in same size. During the transform operation corresponding elements of each matrix is divided as shown in (2-4).

$$\frac{35279.4}{8} = 4409 \ldots\ldots\ldots\ldots \text{2-4}$$

Table 2-1: Quantization matrix

8	4	4	8	16	16	32	32
8	8	8	8	16	32	32	32
8	8	8	16	16	32	32	32
8	8	8	16	32	32	32	32
8	8	16	32	32	64	64	32
16	16	32	32	32	64	64	64
32	32	32	32	64	64	64	64
32	64	64	64	64	64	64	64

In Fig. 2-7, all the elements of A_1 are non-zero but after quantization only 14 non-zero values are left. So, instead of sending 64 elements now it is required to transmit only 14 elements which save almost 80% of the total bandwidth. This is how quantization process reduces the transmission power loss.

2.3 Summary

In this chapter, we have discussed the necessity of image compressor for a power limited WCE application, how this compression could be achieved without losing reconstructed image quality and different types of image compression techniques. We have also described different types of color planes and transform coding used in image compression standards. In next chapter, we will present the image compressors that we have designed using these components.

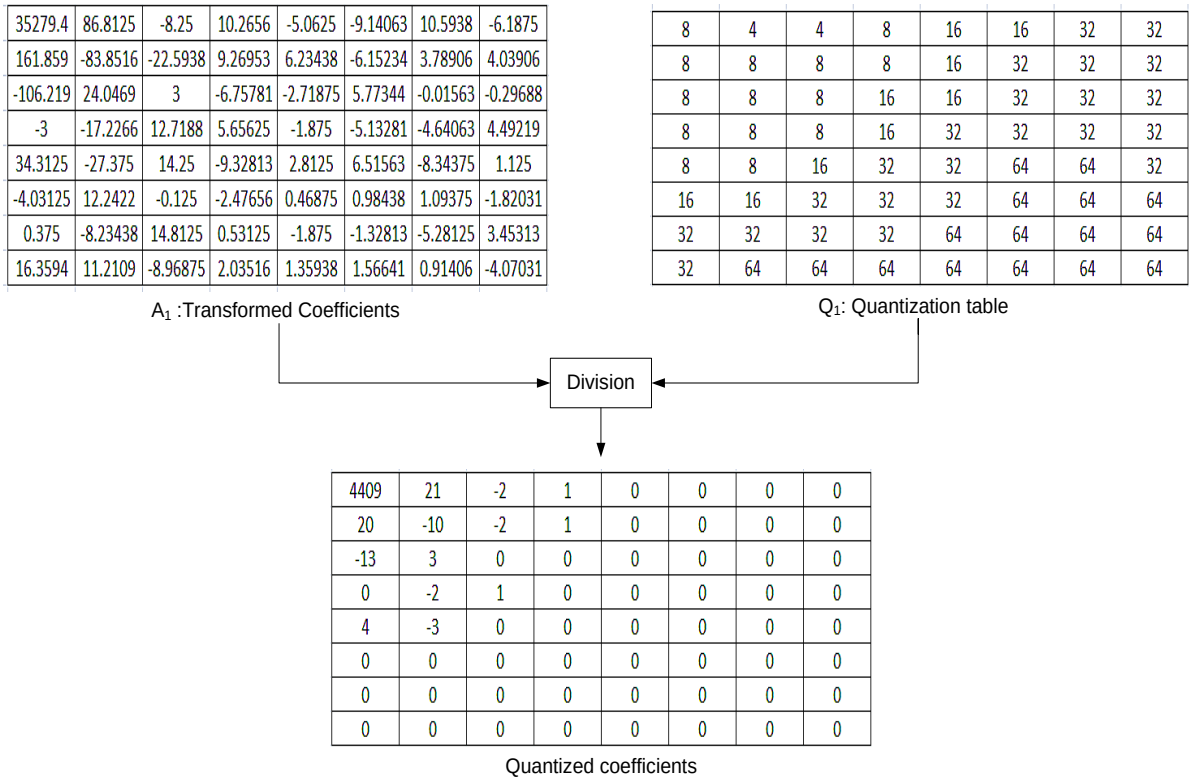

Figure 2-7: Operation of a quantization unit

CHAPTER 3
PROPOSED DESIGNS

Image compressor is a key component in a capsule endoscope (CE). Several criteria have to be fulfilled to design an efficient image compressor for CE. Area is one of such parameters that should keep in mind during CE design because it is difficult for the patient to swallow a big capsule. To keep the capsule size small, only two button batteries can be accommodate inside the CE. So, the image compressor of the CE should be power efficient so that these button batteries can support the CE for the entire examination period (approximate 10 hours [14]).

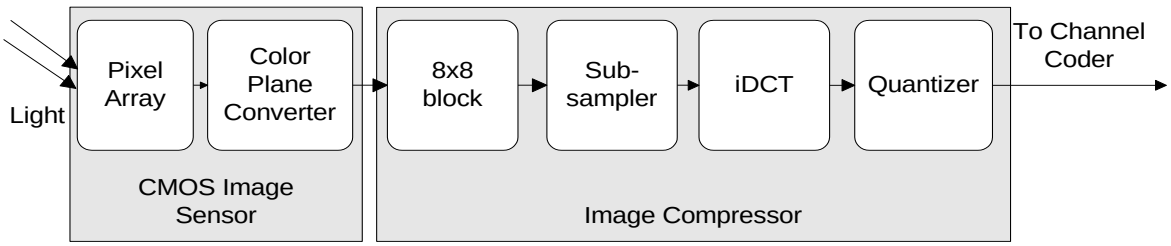

Figure 3-1: Overall block diagram of the proposed designs

Power consumption of an image compressor depends on the computational complexity of the compression process. Different compression algorithms are used to compress images. But most of them are power starving and not suitable for the WCE application. That is why we have tried to design a power efficient image compressor that would be suitable for the WCE application. To achieve high compression, we have chosen lossy compression. High spectral redundancy of endoscopic images permits us to use this lossy compression. In this design we have used the skeleton of the JPEG image compressor and altered its components to achieve the best results. We have started with a simple YUV based design and gradually added complexity to it. All the designs followed the common

structure of Fig. 3-1. Initially subsampler unit was not used in the design to keep the experiment simple. All of the designs were published in different prestigious international conferences [25]-[28].

3.1 Design-1: YUV and DCT-II

Our first experiment has been done with YUV color space and DCT-II. For this experiment, we have collected 12 endoscopic images from [24] which are in RGB format. Endoscopic images are not available in the raw format because all the CEs use some form of lossy compression. However, these images are of very high quality and most researchers are using these images in their experiments.

3.1.1 Color Plane Transform: YUV

At first all the images have been transformed into YUV color space. As was mentioned in the section 2.2.1.1, YUV color space has uncorrelated component; so without affecting the overall reconstruction quality, images could be sufficiently compressed by compressing U and V components. This feature could be explained using the histogram which represents the number occurrence of a particular pixel value in an image. For example, in Fig. 3-2 (a), pixel value of 128 occurred 500 times in red component of an endoscopic image. Histograms of an endoscopic image in both RGB and YUV format have been given in Fig.3-2.

In Fig. 3-2 (a), all red, green, blue components of the RGB format pixel values distribute over the entire range where in Fig. 3-2 (b), pixel values are accumulated in a small

interval for U and V components. So, smaller number of bits could be used to represents these two components with compare to Y component and achieve high compression ratio.

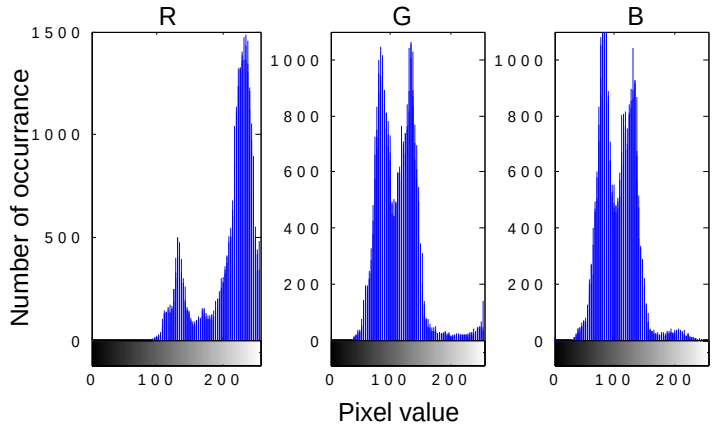

(a) Histogram of an endoscopic image in RGB format

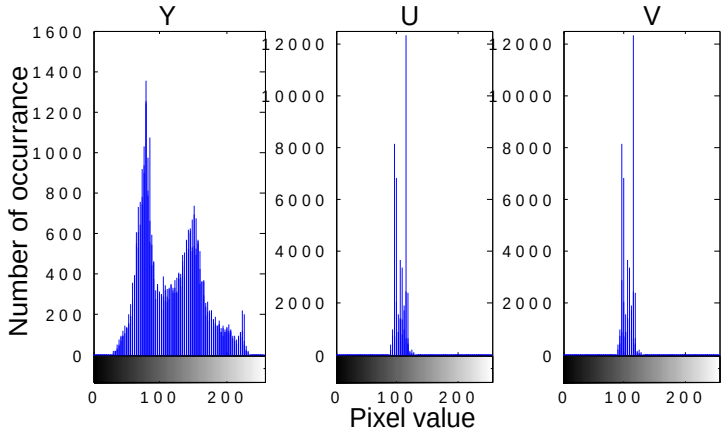

(b) Histogram of an endoscopic image in YUV format

Figure 3-2: Histogram of an image in two different formats

3.1.2 Transform Coding: 8x8 DCT-II

In the second stage, we have divided the image into 8x8 blocks to optimize the compression ratio and reconstruction image quality as we have explained in section 2.2.3.

Then the blocks have been transformed using DCT-II kernel. This was the first stage of this work, so the whole experiment was simulation based. That is why hardware cost of the DCT-II kernel was not considered.

Table 3-1: Quantization matrix for the design-1

(a) Quantization matrix for the Y component

4	2	2	2	2	4	4	4
2	2	2	2	4	4	4	4
2	2	2	4	4	4	4	8
2	2	4	4	4	4	8	16
2	4	4	4	4	8	16	16
4	4	4	4	8	16	16	32
4	4	4	8	16	16	32	32
4	4	8	16	16	32	32	32

(b) Quantization matrix for the U component

8	4	4	8	16	16	32	32
8	8	8	8	16	32	32	32
8	8	8	16	16	32	32	32
8	8	8	16	32	32	32	32
8	8	16	32	32	64	64	32
16	16	32	32	32	64	64	64
32	32	32	32	64	64	64	64
32	64	64	64	64	64	64	64

(c) Quantization matrix for the V component

4	4	4	8	8	8	16	32
4	4	4	8	8	16	32	32
4	4	8	8	16	32	32	32
8	8	8	16	32	32	32	64
8	16	16	32	32	32	64	64
16	16	32	32	32	64	64	64
16	32	32	64	64	64	64	64
16	32	64	64	64	64	64	64

3.1.3 Quantization

After the DCT-II transform, low frequency components were accumulated in the top-left corner of the 8x8 blocks and high frequency components went to the bottom-right corner. As explained in section 2.2.4, human eyes are more sensitive to the low frequencies, so, quantization matrices were designed with smaller entry in the top-left corner and high valued entries otherwise. Based on the analysis in section 3.1.1, we have designed quantization matrices for U and V components, which have discarded all the frequency components for these two color components except a few low frequency components. Quantization matrix for the Y component was less aggressive than the U and V components. Quantization entries were all power of two for low cost implementation. Quantization matrices have been given in Table 3-1. Since blue color is the least dominant component in endoscopic images, quantization matrix of U component has the highest value entries.

The overall block diagram for design-1 is given in Fig. 3-3.

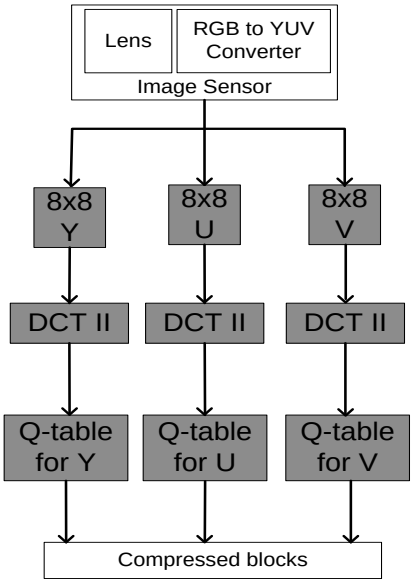

Figure 3-3: Block diagram of the algorithm used in design-1.

3.2 Design-2: YCgCo and Integer DCT

In this second design, we were more concerned about the hardware implementation. So, the choice of color space and transform coding was based on their implementation complexity. In this design, we have tested the efficacy of YCgCo color space and integer DCT (iDCT) with a set of quantization matrices for YCgCo. This was also a simulation based design.

3.2.1 Color Plane Transform: YCgCo

As is described in section 2.2.1.2, YCgCo is a recently introduced color plane with more uncorrelated components than the YUV and RGB color planes. But the main advantage for which this color plane was accepted in this design is its simple implementation. It requires significantly low adder and shifter when compared to YUV to convert one pixel from RGB to YCgCo plane. Hardware comparison of the two color planes to converter one pixel is shown in Table 3-2.

Table 3-2: Comparison of hardware requirement for different converters

	RGB to YUV Converter	**RGB to YCgCo Converter**
No. of adder	25	4
No. of shifter	55	2

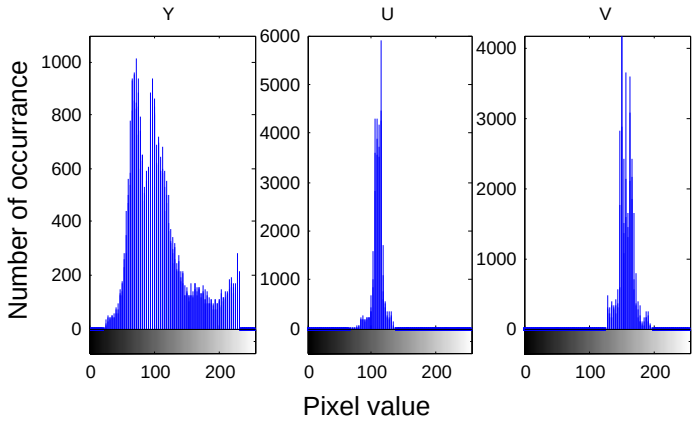

(a) Histogram in YUV format

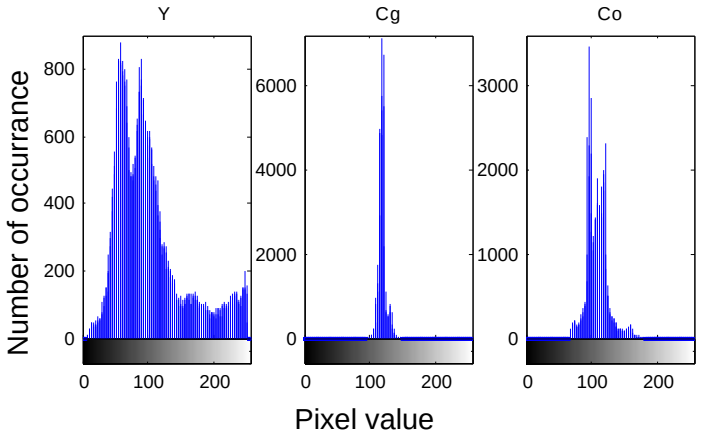

(b) Histogram in YCgCo format

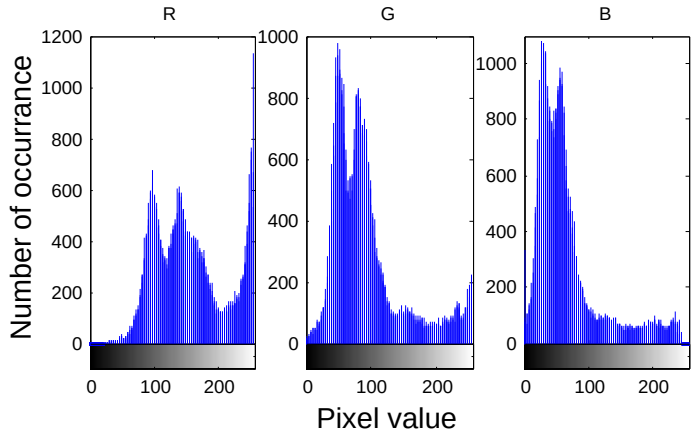

(c) Histogram in RGB format

Figure 3-4: Histogram of an endoscopic image in different color planes

Components of this color plane are also uncorrelated like the YUV plane which was proved by the histogram for an endoscopic image given in Fig. 3-4 in RGB, YUV, YCgCo color plane. It is clear from the histogram that Cg and Co components could be treated as the same way as U and V components of YUV. Histogram of Co component which represents the orange component of the image is wider than the corresponding V component because of the dominance of red component of endoscopic images when Cg (green offset) has the thinnest histogram and allows us to compress heavily without reconstruction quality degradation.

3.2.2 Transform Coding: 8x8 iDCT

In this design, iDCT was used instead of DCT-II to reduce the implementation complexity. Different types of 8x8 iDCT and binary DCT (BinDCT) were described in section 2.2.3. Performance of all these transformation was investigated in this experiment for 12 endoscopic images. Their performance (measured in PSNR which is described in 4.1.1) and hardware cost have been shown in Table 3-3. From the table it was clear that iDCT describe in VC-1[29] showed the best performance in terms of reconstruction image quality and implementation complexity. Here, BinDCT had only 9 shifters, which was lower than the shifter requirement of VC-1. But shifter implementation is easier to than the adder. So, in this design as well as the next designs this transformation was used for the frequency domain transformation.

3.2.3 Quantization

Quantization matrix design approach was the same as the previous design. Based on the properties of the endoscopic images, two quantization matrices were proposed. Light quantization is done for luminance (Y) component since it holds the most significant information and heavy quantization matrix was designed for the green offset (Cg) and orange offset (Co). This aggressive quantization of green and orange component left the reconstructed images remain unaffected because of the statistically uncorrelated components. Quantization matrices used in this design are shown in Tables 3-4.

Table 3-3: Performance comparisons of different 8x8 iDCT

Sample	iDCT in VC-1		BinDCT[19]		BinDCT[20]		iDCT in H.264		iDCT in AVS	
	PSNR (dB)	Hardware Count	PSNR (dB)	Hardware Count	PSNR (dB)	Hardware Count	PSNR (dB)	Hardware Count	PSNR (dB)	Hardware Count
1	50.75	18 Adders and 20 Shifters	44.17	28 Adders and 9 Shifters	42.66	30 Adders and 13 Shifters	41.06	18 Adders and 17 Shifters	42.57	17 Adders and 20 Shifters
2	51.26		45.47		44.26		42.06		43.81	
3	52.48		46.76		44.27		44.74		45.93	
4	51.38		46.21		43.44		42.73		44.37	
5	50.66		44.81		42.45		40.86		42.62	
6	50.56		44.40		42.84		40.99		42.53	
7	50.75		44.51		42.99		41.08		42.76	
8	50.94		45.31		42.50		42.65		44.06	
9	50.82		44.08		43.39		42.27		43.70	
10	51.87		45.31		43.50		42.63		44.56	
11	51.27		45.29		44.82		43.66		44.60	
12	50.81		44.36		42.62		40.15		42.48	

Table 3-4: Quantization matrices used in design-2

(a) Quantization matrix for Y component

8	4	4	8	16	16	32	32
8	8	8	8	16	32	32	32
8	8	8	16	16	32	32	32
8	8	8	16	32	32	32	32
8	8	16	32	32	64	64	32
16	16	32	32	32	64	64	64
32	32	32	32	64	64	64	64
32	64	64	64	64	64	64	64

(b) Quantization matrix for Cg and Co component

16	8	8	16	32	32	64	64
16	16	16	16	32	64	64	64
16	16	16	32	32	64	64	64
16	16	16	32	64	64	64	64
16	16	32	64	64	128	128	64
32	32	64	64	64	128	128	128
64	64	64	64	128	128	128	128
64	128	128	128	128	128	128	128

Overall block diagram for this design has been given in Fig. 3-5.

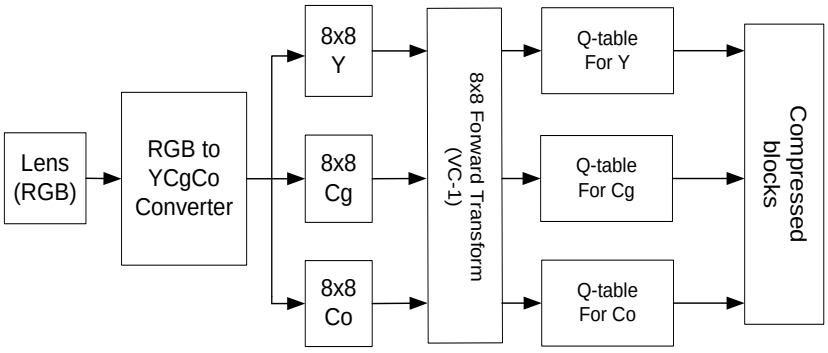

Figure 3-5: Block diagram of design-2

The entries in the quantization matrices are smaller at the top left corner and gradually increased at the bottom right corner to eliminate the less significant AC components. Quantization matrix entries were chosen as the multiple of 2 for efficient hardware implementation.

3.3 Design-3: YEF and Integer DCT

In this work, we have tested this algorithm with a novel color plane, named YEF . This color plane is proposed in [17] where a DPCM based endoscopic image compressor successfully used this color plane. So, in this experiment, we have tested the performance of this color plane for the DCT-based compressor.

In this stage, the design was implemented in Xilinx ISE and area, power and frequency was measured using Synopsys design analyzer. This work is very close to the design-2 except the color plane and few tuning in the quantization matrix based on the properties of YEF color space.

In YEF, the luminance information is stored in Y component, E stores the difference between luminance and green component, and F stores the difference between luminance and blue component. It exploits the features of endoscopic images and more efficiently separates the information in luminance and chrominance components. Thus pixel values of its chrominance components are distributed in a smaller interval than the YUV and YCgCo as is shown in Fig. 3-6. From the histogram it is clear that more compression could be possible for the E and F components without spoiling the reconstruction quality.

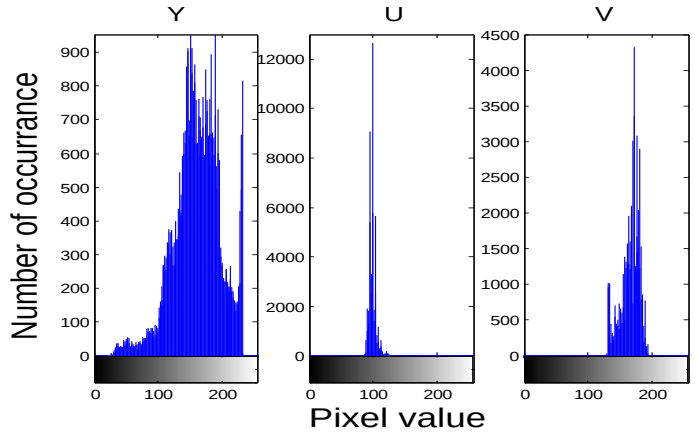

(a) Histogram in YUV format

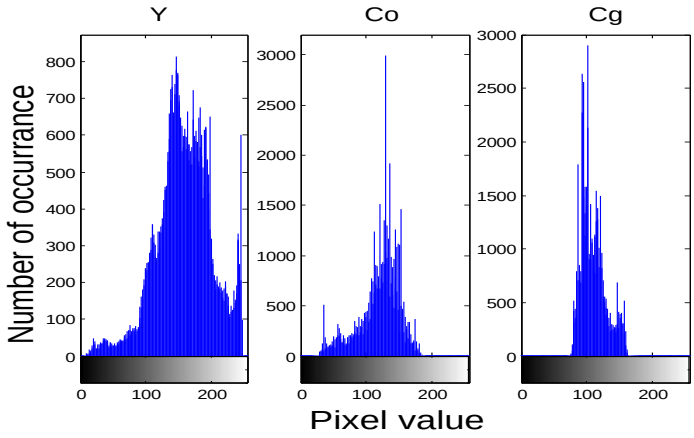

(b) Histogram in YCgCo format

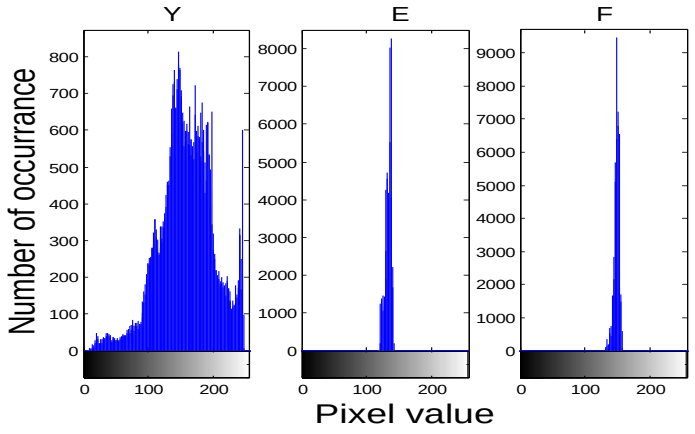

(c) Histogram in YEF format

Figure 3-6: Histogram of an endoscopic image in different color planes

The iDCT described in VC-1 was also used here for the frequency domain transform due to its performance and implementation simplicity as shown in Table 3-3. In YEF color space, E and F components were showing the similar histogram. It was also given in [17] that the standard deviation is also very close for these two components. So, same quantization matrices were used to quantize E and F components. The Quantization matrices used in this design are given in Table 3-5. As before, the Quantization matrix entries were power of 2 and gradually increased from top-left to bottom-right corner.

Table 3-5: Quantization matrices used in design-3

(a) Quantization matrix for Y component

8	4	4	8	16	16	32	32
8	8	8	8	16	32	32	32
8	8	8	16	16	32	32	32
8	8	8	16	32	32	32	32
8	8	16	32	32	64	64	32
16	16	32	32	32	64	64	64
32	32	32	32	64	64	64	64
32	64	64	64	64	64	64	64

(b) Quantization matrix for E and F component

16	8	8	16	32	32	64	64
16	16	16	16	32	64	64	64
16	16	16	32	32	64	64	64
16	16	16	32	64	64	64	64
16	16	32	64	64	128	128	64
32	32	64	64	64	128	128	128
64	64	64	64	128	128	128	128
64	128	128	128	128	128	128	128

3.4 Design-4: Design-2 with Subsample

Based on the performance of the previous designs, we have added subsampling with the image compressor of Design-2 and tested the efficacy of this design for endoscopic images in both Wide Band Imaging (WBI) and Narrow Band Imaging (NBI) format. All our previous designs were for the in WBI but NBI is also an important category of endoscopic images. Images in NBI are captured using some specific narrow band lights thus can provide the visibility of intestinal vessels and mucosal structures over traditional WBI [30]. In Fig. 3-7, an endoscopic image in both NBI and WBI has been shown. It is clear from Fig. 3-7 that vessels are clearer in NBI than WBI.

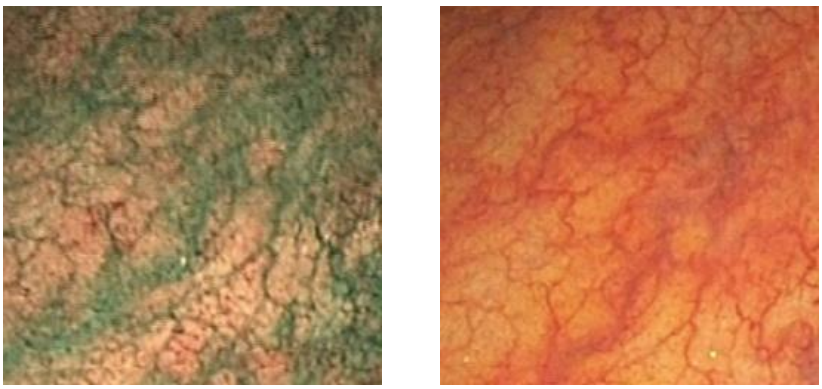

NBI WBI

Figure 3-7: An endoscopic image in WBI and NBI

All our previous designs reconstructed images with more than the required level of reconstruction quality which is found to be 35 dB as noted in [31]. So, subsampling was added to reduce the reconstruction quality in exchange of additional compression. This increase of compression also reduced the power consumption and made this design more competitive with others. This design was also implemented using Xilinx ISE and physical parameters were measured using Synopsys design analyzer.

3.4.1 Color Plane Transform: YCgCo

In this design, more effort was given to reduce the hardware cost to implement the proposed algorithm since the reduction of hardware cost reduces both the power and occupied area. That why we have used YCgCo as it has a bit low implementation cost with compare to YEF and YUV as shown in Table 3-6.

Table 3-6: Comparison of hardware requirement for different converter

	RGB to YUV Converter	**RGB to YCgCo Converter**	**RGB to YEF Converter**
No. of adder	25	4	6
No. of shifter	55	2	9

3.4.2 Subsampling

In this final design, we have added subsampling to achieve better compression in exchange of reconstruction quality drop. As is described in section 2.2.2, chrominance subsampling is an important part of image compression where spectral redundancy is eliminated from the image. From the histograms given in the previous section, it was clear that heavy subsampling is possible for endoscopic images in YCgCo color plane. So, instead of the conventional subsampling, we have used customized subsampling schemes which were only applicable for the endoscopic image compression. A detail of this process was described in section 2.2.2. Compression loss of YCgCo plane over YEF plane is countered using subsampling. Subsampling unit works by discarding some inputs, no addition or

shifting operation was required other than a few wiring for control. So, almost no additional hardware cost was required to implement the subsampling unit.

3.4.3 Transform Coding: 8x8 iDCT

The performance of both iDCT and BinDCT was re-evaluated for the subsampled images because the compression of the DCT based algorithm depends on the likeliness of the neighboring pixel values. By subsampling, neighboring pixels are discarded, so the iDCT that performs well in the design without subsampling may not work for this design. This design was also proposed for the NBIs. So, performances of the transform units for NBIs were also required to be analyzed. Performance of all the iDCT and BinDCT along with their implementation cost in terms of adder and shifter has been shown in Table 3-7 for both the NBIs and WBIs. Here, 8:1:2 subsampling was used. From the table, we found that the iDCT described in VC-1 was still working better than the other DCTs. So, we have used this transformation in this design.

Table 3-7: Comparisons of different 8x8 iDCTs

iDCT Schemes	**PSNR (dB)**		**Hardware Cost**	
	WBI	NBI	Adder	Shifter
BinDCT[19]	39.25	39.71	28	9
BinDCT[20]	38.10	37.87	30	13
H.264	38.79	38.17	18	17
AVS China	39.57	39.40	20	17
VC1	40.64	41.24	18	20

3.4.4 Quantization

Using quantization unit along with the subsampling unit compress the images to reduce the transmission power consumption. Quantization matrices given in Table 3-4 were also used in this design because the same tables also provided the optimum results for the compression algorithm with subsampling scheme.

The overall block-diagram of our final design is given in Fig. 3-8.

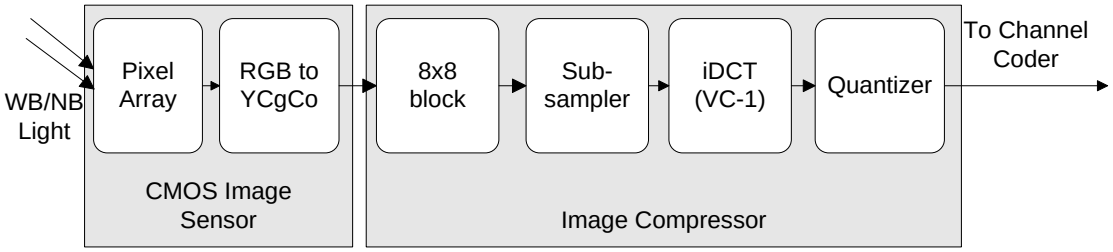

Figure 3-8: Block diagram of the compression algorithm proposed in design-4

3.5 Summary

In this chapter, we have described four different designs for image compressor of the WCE application. The first two designs were simulation based and done to verify the performance of the DCT based image compressor in luminance-chrominance color plane. The last two designs were done to confirm the applicability of the proposed compressor in practical situation. The performance evaluation for these designs will be presented in the next chapter.

CHAPTER 4

PERFORMANCE EVALUATION

The performance evaluation of the proposed has been done using MATLAB 7.0.1. Endoscopic images, collected form [24], have been used in this evaluation. Total 100 endoscopic images were used to generate the results. The purpose of performance assessment of the algorithms was to measure the reconstruction image quality and calculate the compression ratio. Both the indices are important for the CE because high compression saves the transmission power and reconstruction quality is essential for the accurate diagnosis. Several image quality indices were used to assess the performance of these designs. Both the statistical and structural indices were used to obtain a more reliable evaluation results. In first section, the indices that were used to evaluate the performance have been described and results in the next section. As a reference, all the designs described in Chapter 3 have been summarized in Table 4-1.

Table 4-1: Summary of the designs described in Chapter 3

	Color space	**Subsampling**	**Transform type**	**Quantization**	**Type of image**
Design-1	YUV	No	DCT-II	Table 3-1	WBI
Design-2	YCgCo	No	iDCT (VC-1)	Table 3-4	WBI
Design-3	YEF	No	iDCT (VC-1)	Table 3-5	WBI
Design-4	YCgCo	Yes	iDCT (VC-1)	Table 3-4	WBI and NBI

4.1 Image Quality Indices

Image quality indices (IQIs) are the values used to evaluate the quality of a digital image which is subject to distortion due to the acquisition, processing, compression, storage,

transmission and reproduction. Medical images such as endoscopic images are finally examined by a human doctor, so subjective evaluation should be the most reliable method to make decision on the quality of a reconstructed image. But subjective evaluation is very time-consuming and expensive. So, we had to depend on the objective IQIs like most other researchers did.

There are several types of objective indices used in practice. They can be classified into three categories. A full-reference metric considers the distortion free image is available and image quality is evaluated by comparing with the distortion free images. Blind or no-reference metrics are used when the distortion free image is not available. Last category is the reduced-reference metric where transmitter also transmits some vital information regarding the transmitted images along with the coded images. In this simulation we have used the full-reference metrics.

4.1.1 Peak Signal to Noise Ratio (PSNR)

PSNR is the most widely used objective index to evaluate the performance of the reconstructed image. It uses the statistical property, mean square error (MSE) between the original image and the reconstructed image. The error added to the image due to the noise, which was intentionally generated in this work to discard the redundancies. PSNR of a color image could be calculated using (4-1).

$$PSNR = 20 \cdot \log_{10}\left(\frac{MAX}{\sqrt{MSE}}\right) \quad \text{..... (4-1)}$$

Where, $MSE = \frac{1}{3mn}\sum_{l=1}^{3}\sum_{i=0}^{m-1}\sum_{j=0}^{n-1}\left[I_l(i,j) - K_l(i,j)\right]^2$ and $MAX = 255$, for 8-bit per pixel for each component. During MSE calculation, m and n are the dimensions of the image and l represents the number of components in the color space. $I(i,j)$ and $K(i,j)$ are the reference and reconstructed images respectively. All the color spaces we have used in this designs consists of 3 components.

4.1.2 Compression Ratio (CR)

Compression ratio represents how much data is compressed using the compression algorithm with respect to the original image size. So, this metric is an important measurement in image compressor's performance evaluation. Increase of CR is good for WCE application since it reduces the transmission power consumption by the image compressors but at the same time it reduces the reconstructed image quality, so trade off is required between the compression ratio and image quality metrics. In literature, several methods exist to measure the CR. CR for this thesis has been measured using (4-2).

$$CR = \frac{Number\ of\ zeros\ in\ the\ compressed\ image}{Total\ number\ of\ pixels\ in\ the\ original\ image} \times 100\% \quad \ldots\ldots\ldots\ldots \text{(4-2)}$$

4.1.3 Structural Similarity (SSIM) Index

SSIM [32] is an objective IQI which measures the structural similarity between the reference image and the reconstructed image. SSIM gives more reliable results than the MSE based PSNR because human visual system is more dependent on structure of an image.

Several experiments have been done where PSNR fails to show the exact degree of degradation of the original image. Result of one such experiment is given in Fig. 4-1.

(a) Original Image (b) Distorted image {PSNR = 33 dB} (c) Distorted image {PSNR=33 dB}

Figure 4-1: Experiment shows the limitation of PSNR

In Fig 4-1, we can see that both (b) and (c) has the same PSNR but they do not have the same degree of distortion. Such results were the motivation for using structural indices as well as the statistical metrics. In this work, SSIM is calculated as is described in [32].

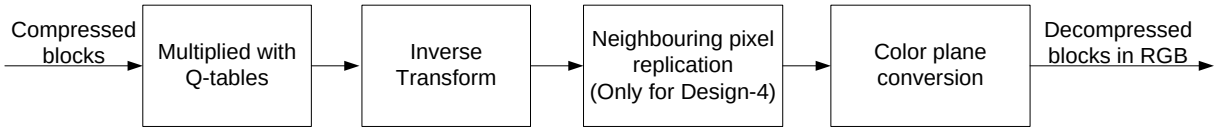

Figure 4-2: Block diagram of the decoding procedure

4.2 Results and Discussion

The performance of these proposed designs has been presented in this section using the IQIs described in section 4.1. We intent to evaluate the performance of the image compressor, so we have ignored the transmission and acquisition distortion added to the

reconstructed images. Compressed image was uncompressed using the reverse procedure. The method that was used to reconstruct the compressed image has been shown in Fig. 4-2.

4.2.1 Design-1

In this design, we have used 12 endoscopic images of different parts of gastrointestinal tract. Performance of the image compressor in YUV and RGB format was compared in Table 4-2. It was clear from the table that, the DCT based compression algorithm worked better in YUV plane than the RGB plane. Performance for each component has been compared in Table 4-3 which showed that overall reconstructed image quality was unaffected due to the heavy quantization of the luminance components. Each components of a sample image in YUV color plane with their PSNR has been shown in Fig. 4-4. Overall PSNR and compression ratio of that image in RGB format has been given in Fig. 4-3. In both figures original and reconstructed images were perceptually indistinguishable, thus proved the success of the YUV-based compression algorithm.

(a) Original

(b) Reconstructed
CR= 89.95%, PSNR = 47.81dB

Figure 4-3: Original and reconstructed endoscopic image in RGB using design-1

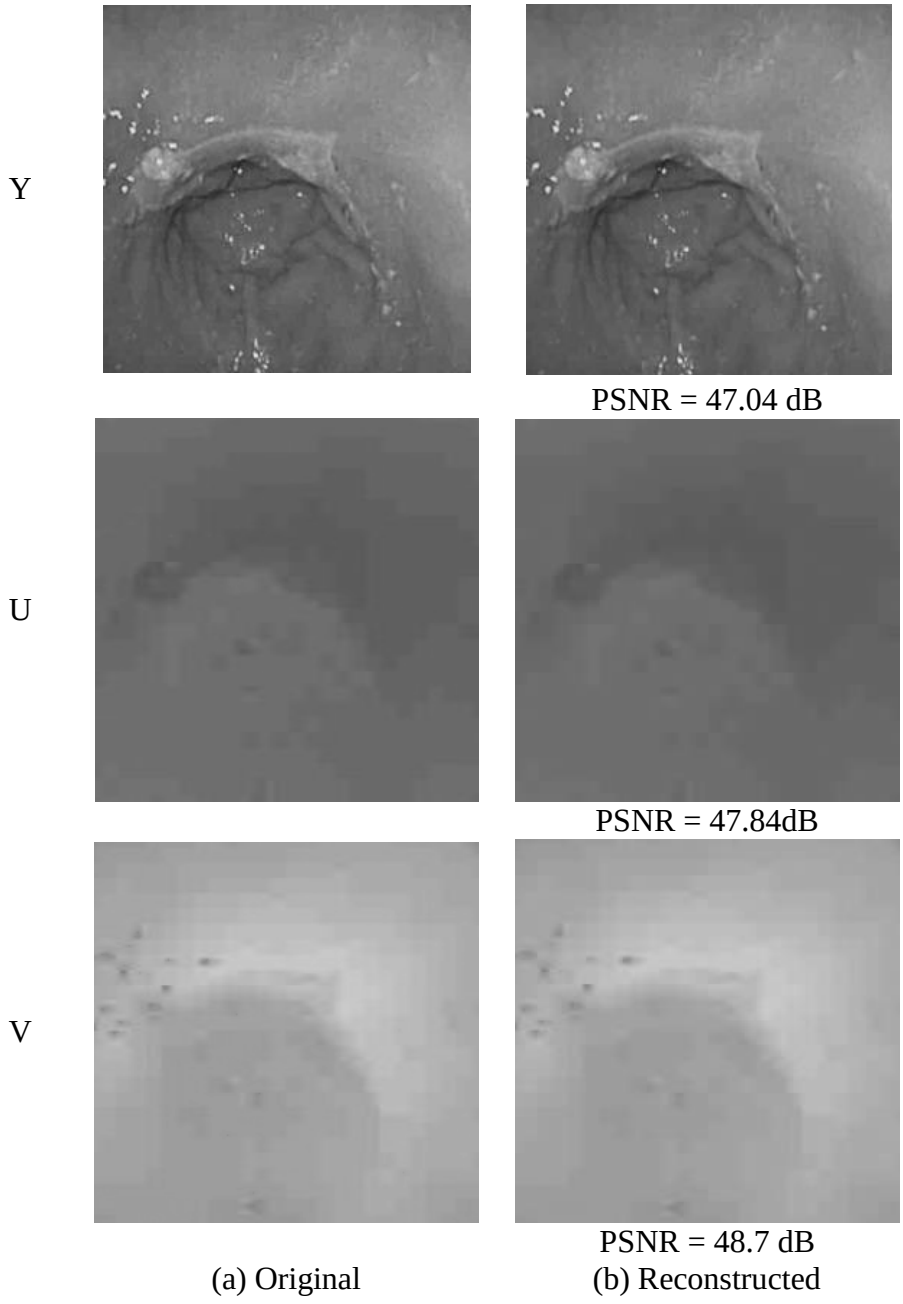

Figure 4-4 : Y,U,V components of the original and reconstructed image using design-1

Table 4-2: Performance comparison of YUV and RGB format using the proposed method

Sample	YUV format			RGB format		
	PSNR	SSIM	CR (%)	PSNR	SSIM	CR (%)
1	47.4	0.9909	88.98	39.89	0.9648	82.77
2	47.69	0.9914	90.93	41.49	0.9711	86.16
3	48.43	0.9925	90.17	40.88	0.9578	83.65
4	48.23	0.9919	89.43	40.32	0.9599	82.75
5	47.21	0.9902	88.31	39.58	0.9627	81.53
6	47.27	0.9902	89.31	40.2	0.9672	83.53
7	47.38	0.9905	89.47	40.5	0.9627	83.85
8	47.7	0.9907	87.61	39.29	0.9473	79.92
9	47.56	0.991	89.9	40.99	0.9651	84.48
10	47.81	0.9915	89.95	40.32	0.9615	83.8
11	48.35	0.9913	91.33	42.31	0.9711	86.81
12	47.46	0.9907	89.25	39.75	0.9645	83.09
Avg.	47.71	0.9911	89.55	40.46	0.9629	83.53

Table 4-3: Compression Ratio and Quality of the Reconstructed Images

Sample	PSNR (dB)				SSIM	CR (%)
	Y	U	V	Overall		
1	46.82	47.55	47.89	47.4	0.9909	88.98
2	47.61	47.19	48.35	47.69	0.9913	90.93
3	47.24	48.65	49.77	48.43	0.9925	90.17
4	47.03	48.58	49.44	48.23	0.9919	89.43
5	46.46	47.32	47.99	47.21	0.9902	88.30
6	46.98	47.07	47.8	47.27	0.9902	89.31
7	46.97	47.33	47.9	47.38	0.9905	89.47
8	46.36	48.07	49.13	47.7	0.9906	87.61
9	47.4	47.26	48.05	47.56	0.991	89.90
10	47.04	47.84	48.7	47.81	0.9915	89.95
11	47.97	48.09	49.07	48.35	0.9912	91.33
12	46.65	47.90	47.96	47.46	0.9907	89.25
Avg.	47.04	47.74	48.50	47.71	0.9910	89.55

4.2.2 Design-2

In design-2, same 12 images have been used to evaluate the performance of the proposed algorithm. Table 4-4 has showed the component wise results of the reconstructed images in terms of PSNR, SSIM and CR. It was found from the table that Co had a slightly lower PSNR compare to Cg because the same quantization matrix was used for both of them but Co contained more information than the Cg. Original and reconstructed version of a sample endoscopic image has been presented in Fig. 4-5 with their IQIs for each components. In Fig. 4-6, original and reconstructed endoscopic image in RGB format has been shown. Reconstructed images were also barely distinguishable from the original images for this design.

Table 4-4: Performance Evaluation of design-2

Sample	**PSNR(dB)**				**SSIM**	**CR(%)**
	Y	**Co**	**Cg**	**Overall**		
1	51.94	49.95	50.57	50.75	0.9958	77.64
2	51.98	51.03	50.84	51.26	0.9959	80.57
3	53.16	52.39	51.98	52.48	0.9961	80.30
4	52.01	51.36	50.84	51.38	0.9956	78.54
5	51.54	50.20	50.36	50.66	0.9956	76.70
6	51.59	49.94	50.33	50.56	0.9957	77.62
7	52.27	49.79	50.54	50.75	0.9958	78.24
8	51.65	50.68	50.57	50.94	0.9951	76.33
9	51.45	50.28	50.80	50.82	0.9958	79.11
10	53.06	51.38	51.38	51.87	0.9961	80.07
11	52.99	50.33	50.91	51.27	0.9956	79.98
12	51.68	50.15	50.72	50.81	0.9957	77.46
Avg.	52.11	50.62	50.82	51.13	0.9957	78.55

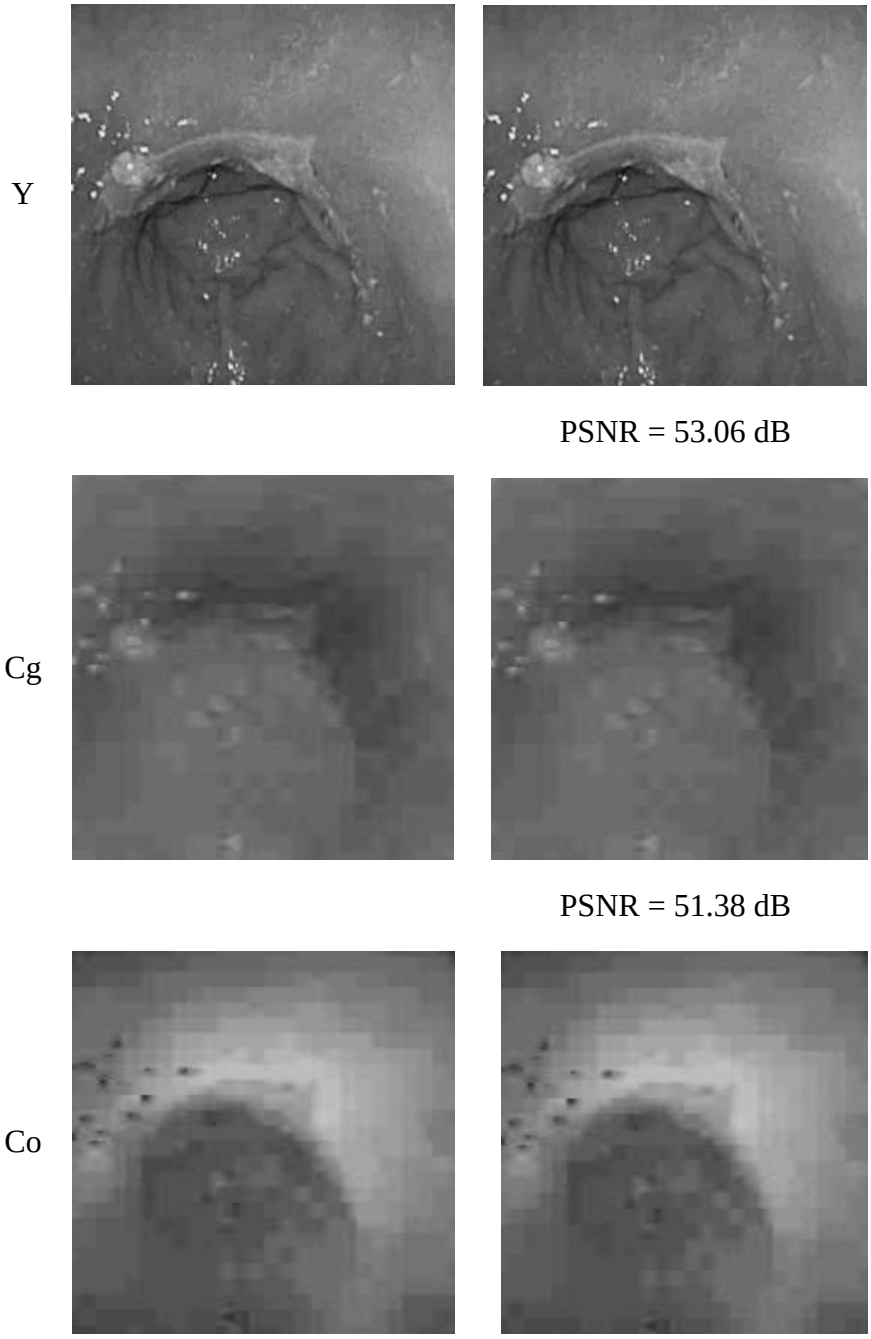

Figure 4-5: Y,Cg, Co components of the original and reconstructed image using design-2

RGB

(a) Original

(b) Reconstructed

CR= 80.07%; PSNR = 51.87 dB

Figure 4-6: Original and reconstructed endoscopic image in RGB format using design-2

4.2.3 Design-3

Performance assessment for the design-3 has been presented in this section. To keep the consistency, results were generated for the same set of 12 images. Component wise indices have been presented in Table 4-5 to demonstrate the effect of different quantization for luminance and chrominance components. Results showed that PSNR did not reduce significantly for the chrominance components as was expected. Perceptually evaluation has been done using the original and reconstructed images given in Fig. 4-7 and Fig. 4-8.

RGB

(a) Original

(b) Reconstructed

CR= 84.27%; PSNR = 54.44 dB

Figure 4-7: Original and reconstructed endoscopic image in RGB format using design-3

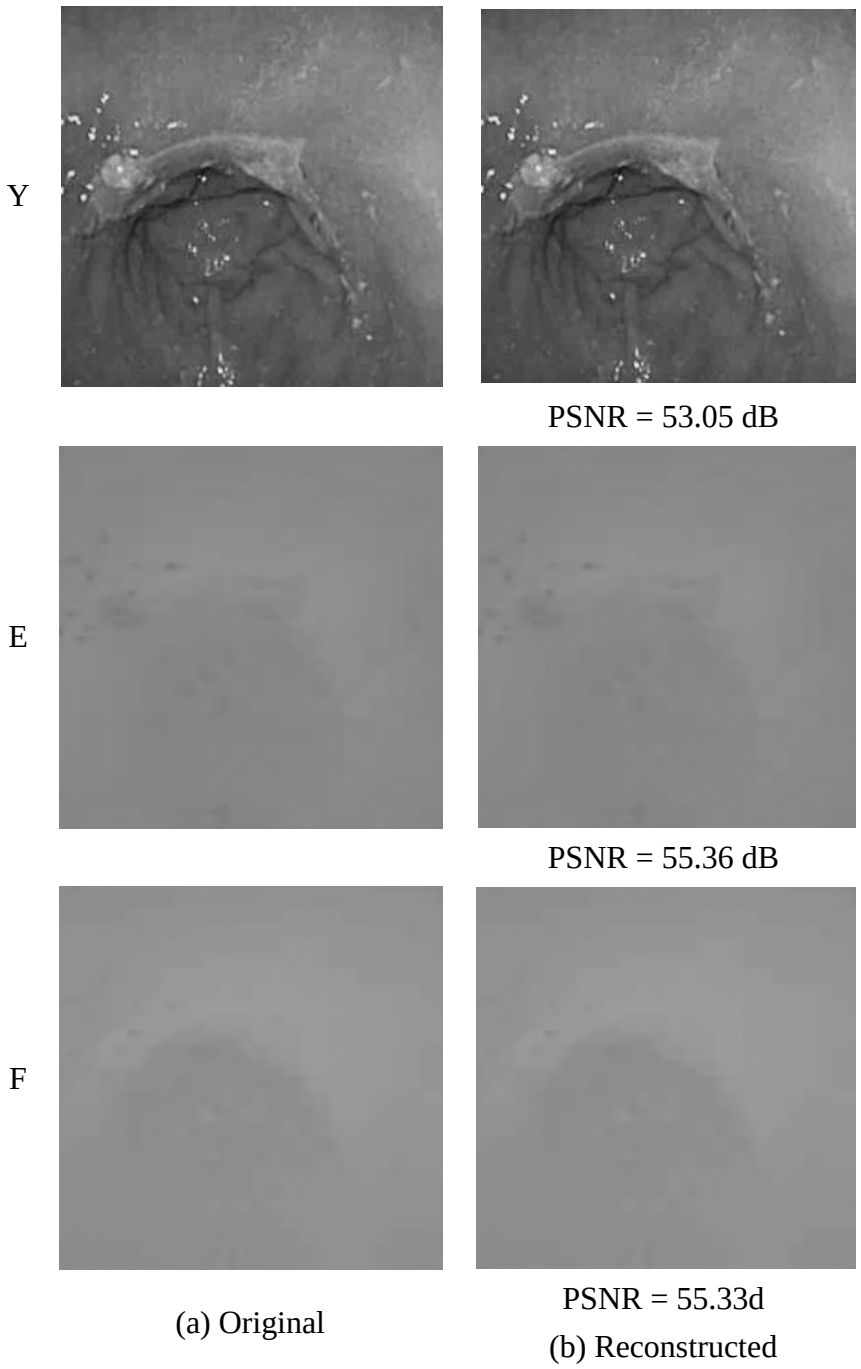

Figure 4-8: Y, E, F components of the original and reconstructed image using design-3

Table 4-5: Performance Evaluation of design-3

Sample	PSNR(dB)				SSIM	CR(%)
	Y	E	F	Overall		
1	51.85	54.42	54.27	53.34	0.9974	82.87
2	52.00	55.34	54.95	53.83	0.9977	84.95
3	53.23	56.11	57.07	55.15	0.9980	84.55
4	51.88	55.32	55.78	53.96	0.9977	83.40
5	51.48	54.40	54.17	53.14	0.9973	82.06
6	51.52	54.48	54.06	53.14	0.9974	82.99
7	52.16	54.54	54.34	53.54	0.9974	83.41
8	51.57	54.69	54.64	53.37	0.9974	81.68
9	51.25	54.86	54.63	53.24	0.9975	83.92
10	53.05	55.36	55.33	54.44	0.9977	84.27
11	52.84	54.52	54.22	53.80	0.9973	85.06
12	51.47	54.34	54.81	53.28	0.9974	82.98
Avg.	52.03	54.87	54.86	53.69	0.9975	83.51

4.2.4 Design-4

Design-4 was evaluated for both WBI and NBI. Results for different subsampling schemes were presented for WBI in Table 4-6. Effect of different subsampling for the NBI was demonstrated in Table 4-7. Analyzed the results, YCgCo812 subsampling has been chosen for the hardware implementation because it optimized the CR and PSNR. Original and reconstructed version of an endoscopic image in both WBI and NBI has been shown in

Fig. 4-9 to demonstrate the performance of the subsample base algorithm. Close similarity of the original and reconstructed image proved the efficacy of the subsample based algorithm.

Table 4-6: Results of NBI images on YCgCo plane

Scheme	**Luminance (Y)**		**Chrominance**		**CR (%)**
	SSIM	***PSNR***	***PSNR***	***PSNR***	
YCgCo844	0.989	51.22	46.89	47.65	80.41
YCgCo824	0.977	51.22	46.89	42.94	80.99
YCgCo814	0.956	51.22	46.89	38.74	81.68
YCgCo822	0.967	51.22	40.92	42.94	81.67
YCgCo812	0.946	51.22	40.92	38.74	82.36
YCgCo811	0.926	51.22	35.79	38.74	83.09
YCgCo16.1.2	0.904	51.22	35.79	35.91	83.57
YCgCo16.1.1	0.889	51.22	32.19	35.91	84.08

Table 4-7: Results of WBI images on YCgCo plane

Scheme	**Luminance (Y)**		**Chrominance**		**CR (%)**
	SSIM	***PSNR***	***PSNR***	***PSNR***	
YCgCo844	0.991	52.45	46.54	47.55	82.50
YCgCo824	0.983	52.45	46.54	42.87	83.10
YCgCo814	0.968	52.45	46.54	38.33	83.80
YCgCo822	0.974	52.45	40.19	42.87	83.83
YCgCo812	0.959	52.45	40.19	38.33	84.53
YCgCo811	0.943	52.45	34.89	38.33	85.27
YCgCo16.1.2	0.928	52.45	34.89	35.01	85.75
YCgCo16.1.1	0.916	52.45	31.03	35.01	86.28

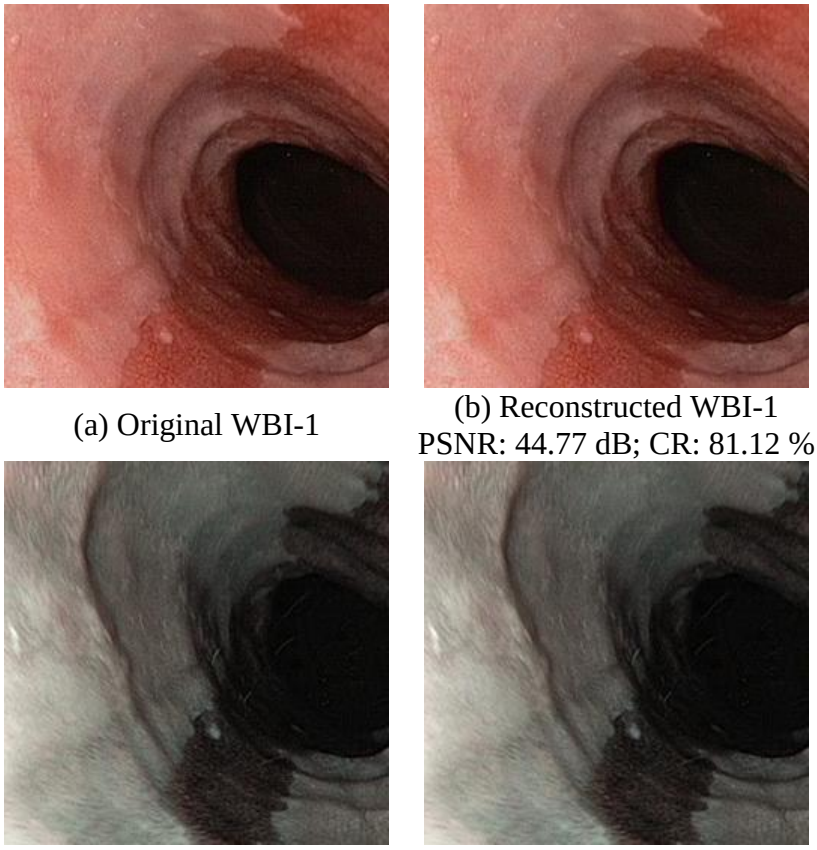

(a) Original WBI-1

(b) Reconstructed WBI-1
PSNR: 44.77 dB; CR: 81.12 %

(c) Original NBI-1

(d)Reconstructed NBI-1
PSNR: 46.93 dB; CR: 82.46 %

Figure 4-9: Original and reconstructed (YCgCo812) images using design-4

Finally, results of the proposed designs were compared with some existing works in Table 4-8. Most of the works are based on the RGB color plane because they wanted to save the implementation cost of the color plane converter. In our design, we have used some easily implementable color plane converters. So, by using a luminance-chrominance color plane instead of RGB color plane, we could achieve more compression in exchange of small hardware cost.

The average of total 100 images has been presented in this table. For design-4, YCgCo812 subsampling was used. Data of this table showed that design-1 was more promising than the others but it has been explained in the previous chapter that this design

was not suitable for hardware implementation. Since our end goal was to obtain high CR keeping the PSNR safe than the minimum threshold of 35 dB [31], we have chosen design-3 and design-4 for hardware implementation.

Table 4-8: Comparison with other works

	Transform Method	**Color Plane**	**Sub-sampling**	**WBI**		**NBI**	
				CR(%)	**PSNR(dB)**	**CR(%)**	**PSNR(dB)**
X. Chen *et al.* [15]	JPEG-LS	RGB	No	56.70	46.43	-	-
K. Wahid *et al.* [33]	DCT	RGB	No	87.13	32.95	-	-
P. Turcza *et al.* [34]	DCT	RGB	No	32.00	36.49	-	-
M. Lin *et al.* [35]	DCT and LZ77	RGB	No	79.65	32.51	-	-
C. Cheng *et al.* [36]	DCT	RGB	No	81.50	31.50	-	-
C. Hu *et al.* [37]	Wavelet Coding	RGB	No	71.98	39.64	-	-
J. Wu *et al.* [38]	Block-based CS	RGB	No	50.00	31.02	-	-
L. Dung *et al.* [39]	H.264-based DCT	RGB	No	82.09	36.24	-	-
T. Khan *et al.* [17]	DPCM	YEF	Yes	80.40	43.70	-	-
T.Khan *et al.* [40]	DPCM	YUV	Yes	80.00	48.00	-	-
Design-1 [25]	DCT-II	YUV	No	90.17	48.43	-	-
Design-2 [26]	iDCT	YCgCo	No	80.30	52.48	-	-
Design-3 [28]	iDCT	YEF	No	82.73	53.80	-	-
Design-4[27]	iDCT	YCgCo	Yes	84.53	40.64	82.36	41.24

4.3 Summary

In this chapter, we have presented all the MATLAB generated results for the designs shown in Table 4-1. Both the IQIs and perceptual evaluation proved that the proposed designs were suitable for CE. VLSI implementation results and battery run-time of the capsule with design-3 and design-4 will be present in the next chapter.

Chapter 5

HARDWARE IMPLEMENTATION

The hardware implementation of design-3 and design-4 is described here. Both designs were modeled using Verilog. A total of 646 lines of Verilog code was written in 9 modules and verified using Xiling ISE. Power, area, frequency were measured using Synopsys design analyzer with 0.18 μm CMOS technology. Same hardware architecture was used to implement these two designs.

5.1 Hardware Architecture

During the system modeling, it was considered that the image was stored in a SRAM and the desired pixels were passed to the image compressor for processing. A universal bridge interface as is described in [41] could be used to access the pixels. Whole architecture used to implement the designs is shown in Fig. 5-1. The hardware architecture of the proposed designs consists of seven major components.

5.1.1 Color Plane Converter

Color plane converter is the first component of the hardware architecture. In the color plane converter, color plane conversion equations as described in section 2.2.1.2 and 2.2.1.3 were implemented to convert the RGB pixels values into YCgCo or YEF. At each clock cycle, one column of the 8x8 block was entered in the conversion unit and converted values were passed to the next unit.

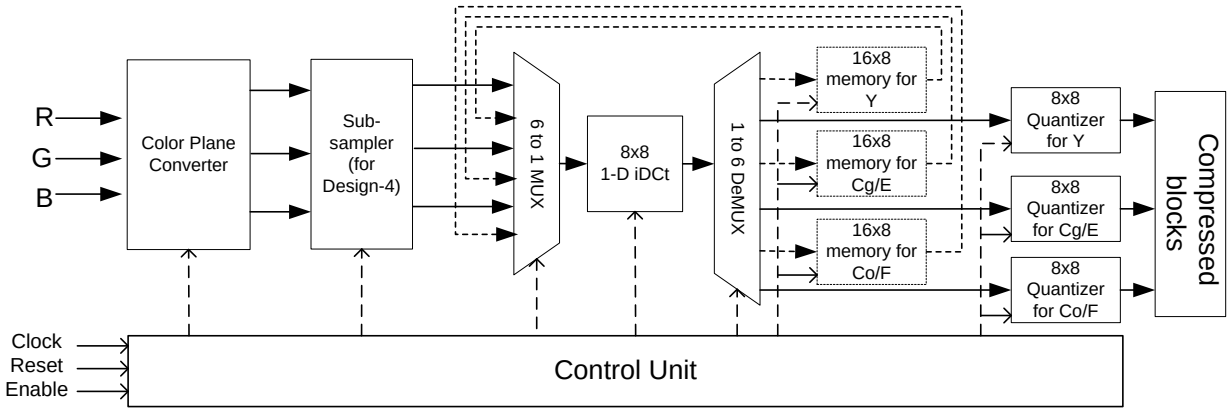

Figure 5-1: Hardware architecture of the proposed image compressor

5.1.2 Subsampler

This unit was only used in design-4. Subsampler unit discard some pixels of Cg and Co components according to the subsampling scheme. Here we have implemented YCgCo812 subsampling scheme. So, using the control signal this subsampler allowed 1 out of 8 pixels for Cg component and 1 out of 4 pixels for Co component to pass to the next unit.

5.1.3 Multiplexer/ De-multiplexer

One multiplexer and one de-multiplexer were used before and after the transform unit. They controlled the access of pixel entry into the transform unit. The multiplexer unit chose one pixel set out of six (three new pixel sets and three 1-D transformed pixel sets). The de-multiplexer unit directed the transformed pixels either to the transpose memory or to quantizer unit. 1-D transformed pixels passed to the transpose unit and the 2-D transformed pixels passed to the quantizer unit. Both the multiplexer and the de-multiplexer units are controlled by the control signal generated by the control unit.

5.1.4 Transform Unit

From section 2.2.3, it was known that total transform operation could be done using two matrix multiplications. We have implemented a 1-D transform unit which could perform one matrix multiplication. This 1-D multiplication was done using adder and shifter to reduce the hardware complexity. These 1-D transformed pixels were transposed and again feed into the transform unit to complete the second multiplication. The multiplexer and the de-multiplexer described in the previous section helped to control this pixel movement.

5.1.5 Quantizer Unit

Three quantizer units were used for three color components. The quantization matrices presented in Table 3-4 and 3-5 were implemented in this unit for design-4 and design-3 respectively. To reduce the hardware complexity, all the coefficients of these tables were power of 2. So, the quantizer unit has done some left-shift operation based on the quantization matrix entry.

5.1.6 Transpose Memory

Transpose memory unit is the essential component for a DCT-based compressor. From (2-9), it was clear that the input for the second multiplication should be transposed before passing to the transform unit. The transpose memory block did this operation. It stored the 1-D transformed columns as row and when a full 8x8 block was stored, it sent the columns to the transform unit. In this simulation, we have implemented them as SRAM but memory synthesizer was not available in our lab. So, power, frequency and area could not be

calculated with this transpose memory. The memory unit and the corresponding wires are marked by dashed lines in Fig. 5-1.

5.1.7 Control Unit

Control unit generated control signals for the entire operation. It combined the signal received as clock, reset and enable and generated the control signal for each components of this hardware architecture. Some simple combinational logic units were used inside this control unit.

5.2 Results and Comparison

To compare the efficiency of the proposed designs, area, power and frequency were measured using Synopsys design analyzer. Approximate runtime for the CE with our designs were also calculated and presented in Table 5-2.

5.2.1 Hardware Cost

Area, power and frequency are three critical parameters required to determine the efficiency of a CE. Using the Synopsys Design Analyzer, we have calculated these results for our proposed designs. The results are summarized in Table 5-1 and compared with other available results. From the table it is clear that our designs are more efficient than others. However, our design did not use entropy encoder, so the performance may change when the comparison will be done with the entropy encoder. It should be noted that, the proposed compressors could compress 256x256 images at 10 fps while power consumption was still

very low. Using the low cost color converter, multiplication free iDCT and hardware friendly quantization matrix was the reasons behind this performance edge. As was expected in Chapter 3, design-4 showed better results than the design-3 in terms of power and area. So, design-4 is the ultimate image compressor proposed in this work.

Table 5-1: Comparison of hardware cost in VLSI

	Area (μm^2)	**Frequency (MHz)**	**Power (mW)**	**Frame rate (fps)**
GICam image compressor[35]	390 k	12.58	14.92	2
K.Wahid et al.[33]*	325 k	150	10	-
M. Lin et al [42]	318 k	7.96	9.17	2
Design-3*	217.29 k	2.50	5.85	10
Design-4*	209.51 k	2.50	3.5	10

* without transpose memory

5.2.2 Estimation of Battery Runtime

The key advantage of the proposed schemes is higher compression ratio and low power consumption. The combination of these two features led to higher battery life, which is a key design constraint in WCE applications. In Table 5-2 , we show battery lifetime comparison with some existing designs of WCE compressors for 256x 256 GI images with 10 fps frame rate (8bpp). In this calculation, we have used the power consumption of an efficient RF transmitter, dedicated for WCE, which could transmit each bit for 1nJ energy

[43]. The power dissipation for LEDs was taken as 2 mW [33]. The average capacity of one battery used in the capsule was taken as 70 mAh @ 1.55 V (two such batteries are considered [33]). Power consumption for the transpose memory was taken as 5.29 mW from [42]. It can be seen from Table 5-2 that the proposed compressor of design-4 resulted in the longest battery life ((70 x1.55x 2) / 13.2 mW ≈ 16.5 hours).

Table 5-2: Comparison of battery life time

Scheme	**Battery lifetime (hours)**
GICam image compressor [35]	10.24
M. Lin et al. [42]	15.77
Design-3	13.79
Design-4	16.41

5.3 Summary

The hardware architecture that is used to implement the designs has been described in the first section of this chapter. The results of the both designs were compared with some existing work in the second section. Comparison results shows that both the design-3 and design-4 worked better than the existing works and design-4 is the most efficient in terms of power, area and frequency. Design-4 met all the necessary criteria required for an efficient image compressor for WCE. Conclusion of the whole thesis and suggestion for some improvements of this work will be presented in the next chapter.

Chapter 6
SUMMARY AND FUTURE WORK

6.1 Summary of Accomplishment

The purpose of this work was to design an image compressor for the area and power limited WCE. We have started with a JPEG-like structure and experimented with several different modules. Experiments were done using four combinations of these components. The object was to design an image compressor with high compression ratio and acceptable PSNR.

The choice of color plane converter, transform unit and subsampling unit were the main factors behind the design. The idea of using the luminance-chrominance based color plane came from the analysis of endoscopic images. Non-uniform distribution of energy in the luminance-chrominance color plane components was the motivation of using such color plane in the image converter design. YUV, YEF, YCgCo were the three color planes used in the experimental designs. Finally, the best performance was achieved from the YCgCo color plane.

An iDCT based transform unit was used in image compressor design. In an effort to keep the implementation cost low, hardware cost was calculated along with the PSNR and CR for different iDCTs. Initially, DCT-II was used in the experiment, but later due to its high complexity, it was not considered in other designs. The iDCT described in VC-1 video coder was finally chosen due to its high PSNR and CR with low implementation cost.

Subsampling was used in the last design which is a common approach of compressing images. Several unconventional subsampling schemes were used to exploit the special features of endoscopic images. Based on the performance, YCgCo812 subsampling scheme

has been chosen for the final implementation, where all the Y components of a 8x8 block have been taken but for Cg, 1 out of 8 columns has been taken and for Co, 1 out of 4 columns has been taken for compression. Adding subsampling increased CR in exchange of PSNR reduction. However, PSNR was not below the acceptable level of 35 dB [31].

Finally, it is shown that the proposed compression scheme satisfies all the requirement of CE in terms of image reconstruction quality, power consumption and occupied area. The design has also been shown to have efficient and improved performance compared to other existing works.

6.2 Recommendation for Future Work

In this section, we have given some recommendations to improve the design which was beyond the scope of the thesis.

1. In the image compressor design, quantization unit was designed to exploit some limitations of HVS. Coefficients of the quantization matrix were selected for easy implementation. But no algorithm was used to generate quantization matrices. Some algorithms were found in [44]-[46] but they need some modification to exploit the features of endoscopic images. Still now, no dedicated quantization matrix generation algorithm is developed for the endoscopic images. So, in future, a quantization matrix generation algorithm could be developed for endoscopic images and used in the image compressor design.

2. Transpose memory is an integral part of the DCT based algorithm. Area and power calculation of our work was done without the transpose memory block because of the unavailability of the memory compiler. In future, more accurate power, area and frequency

calculation could be done by incorporating the power and area requirement of the memory block.

3. Most of the CE image compressors reported in the literature used entropy encoder as the integrated part of the image compressor. However, no entropy encoding was used in our designs. An efficient entropy encoder could be chosen and added to our proposed image compressors.

4. Finally, performance of an image compressor can be accurately evaluated when a prototype is developed and tested in a real situation. So, this image compressor could be implemented in a CE prototype in the future for real world performance analysis.

REFERENCES

[1] Yih K. Tan and John W.L. Fielding, “Early diagnosis of early gastric cancer," European Journal of Gastroenterology & Hepatology, vol. 18, pp. 821–829, 2006.

[2] B. S. Lewis, "Small intestinal bleeding," Gastroenterology Clinics of North America, vol. 29, pp. 67-95, 2000.

[3] G. R. Zuckerman, C. Prakash, M. P. Askin, and B. S. Lewis, "AGA technical review on the evaluation and management of occult and obscure gastrointestinal bleeding," Gastroenterology, vol. 118, pp. 201-221, 2000.

[4] Howarth DM, Tang K, and Lees W, "The clinical utility of nuclear medicine imaging for the detection of occult gastrointestinal haemorrhage," Nucl Med Commun, vol. 23, pp. 591-594, 2002.

[5] R. Eliakim, A. Suissa, K. Yassin, D. Katz, and D. Fischer, "Wireless capsule video endoscopy compared to barium follow-through and computerised tomography in patients with suspected Crohn's disease--final report,” Digestive and Liver Disease, vol. 36, pp. 519-522, 2004.

[6] G. Iddan, G. Meron, A. Glukhovsky, and P. Swain, "Wireless capsule endoscopy,” Nature, vol. 405, pp. 417-417, 2000.

[7] G. D. Meron, "The development of the swallowable video capsule (M2A),” Gastrointestinal Endoscopy, vol. 52, pp. 817-819, 2000.

[8] P. Swain, G. Iddan, G. Meron, and A. Glukhovsky, "Wireless capsule endoscopy of the small-bowel. Development, testing and first human trials," Biomonitoring and Endoscopy Technologies, vol. 1, pp. 19-23, 2001.

[9] O. Co., "Olympus Launches High-resolution Capsule Endoscope in Europe," 2008.

[10] Z. Liao, F. Li, and Z.-S. Li, "Clinical Application of OMOM Capsule Endoscopy in China: A Review of 1,068 Cases," Gastrointestinal Endoscopy, vol. 67, pp. AB265, 2008.

[11] F. Cavallaro et al., "Feasibility, safety and diagnostic yield of OMOM CE, a new capsule endoscopy system," Digestive and Liver Disease, vol. 42, Supplement 2, pp. S164-S165, 2010.

[12] S. Bang et al., "First clinical trial of the "Miro"capsule endoscope by using a novel transmission technology: electric-field propagation," Gastrointestinal Endoscopy, vol. 69, pp. 253-259, 2009.

[13] J. Y. Park, et al., "Multicenter Clinical Experience of the MiRo Capsule Endoscope," Gastrointestinal Endoscopy, vol. 69, pp. AB194, 2009.

[14] J L Toennies,G Tortora,M Simi, P Valdastri, and R JWebster III,"Swallowable medical devices for diagnosis and surgery: the state of the art," Journal of Mechanical Engineering Science, vol. 224, pp.1397-1414, 2009.

[15] X. Chen, et al., "A wireless capsule endoscope system with low power controlling and processing ASIC," IEEE Transactions on Biomedical Circuits and Systems, vol. 3, no 1, pp. 11-22, 2009.

[16] R. Kam and P. Wong, “Customized JPEG compression for grayscale printing,” in Proc. of IEEE Data Compression Conference, pp. 156–165, 1994.

[17] T. H. Khan and K. Wahid, “Low complexity color-space for capsule endoscopy image compression,” IET Electronics Letters, vol. 47, no. 22, pp. 1217-1218, 2011.

[18] H. S. Malvar and G. J. Sullivan, “Transform, Scaling & Color Space Impact of Professional Extensions,” ISO/IEC JTC1/SC29/WG11 and ITU-T SG16 Q.6 Document JVT-H031, Geneva, 2003.

[19] J. Liang, T. D. Tran, “Fast Multiplierless Approximations of the DCT with the Lifting Scheme,” IEEE Transaction on Signal Processing, vol. 49, no. 12, 2001.

[20] T. D. Tran, “The BinDCT: Fast Multiplierless Approximation of the DCT,” IEEE Signal Processing Letters, vol. 7, no. 6, 2000.

[21] M. Narayan, (2007, May 8). Image Coding Fundamental. Available: http://videocodecs.blogspot.ca/2007/05/image-coding-fundamentals_08.html.

[22] Microsoft Corporation, (2004, April 08). Converting Between YUV and RGB. Available: http://msdn.microsoft.com/en-us/library/ms893078.aspx.

[23] D.O. Faigel and D.R. Cave, Capsule Endoscopy, Saunders Elsevier, 2008.

[24] Gastrolab (2010). Available: http://www.gastrolab.net.

[25] A. Mostafa, K. Wahid, and S. B. Ko, “An efficient YUV based image compression algorithm for wireless capsule endoscopy,” in Proc. of Canadian Conference on Electrical and Computer Engineering, pp. 943-946, 2011.

[26] A. Mostafa, K. Wahid and S.B. Ko, “An efficient YCgCo-based image compression algorithm for wireless capsule endoscopy,” in Proc. of International Conference on Computer and Information Technology, pp. 219 - 222, 2011.

[27] A. Mostafa, K. Wahid and S.B. Ko (in press), “A Low-Power Subsample-based Image Compression Algorithm for Capsule Endoscopy ,” in Proc. of International Symposium of Circuits and Systems, in press, 2012.

[28] A. Mostafa, T. H. Khan, S.B. Ko and K. Wahid, “Efficient color space-based compression scheme for endoscopic images,” in Proc. of Information Science, Signal Processing and their Application, in press, 2012.

[29] Sullivan, Gary J. "DirectX Video Acceleration Specification for Windows Media Video v8, v9 and vA decoding (Including SMPTE 421M "VC-1")". Microsoft Corporation, 2007.

[30] L. Song, et. al. “Narrow band imaging and multiband imaging,” Gastrointestinal Endoscopy, pp. 581 - 589, 2008.

[31] R. Istepanian, N. Philip, M. Martini, N. Amso, and P. Shorvon, “Subjective and objective quality assessment in wireless teleultrasonography imaging,” in Proc. of

International Conference of the IEEE Engineering in Medicine and Biology Society, pp. 5346 – 5349, 2008.

[32] Z. Wang, et al., “Image quality assessment: From error visibility to structural similarity,” IEEE Transaction on Image Processing, vol. 13, no 4, pp. 600-612, 2004.

[33] K. Wahid, S.B. Ko, D. Teng, “Efficient hardware implementation of an image compressor for wireless capsule endoscopy applications,” in Proc. of International Joint Conference on Neural Networks, pp. 2761-2765, 2008.

[34] P.Turcza, T. Zieliński, M. Duplaga, “Hardware Implementation Aspects of New Low Complexity Image Coding Algorithm for Wireless Capsule Endoscopy,” in Proc. of the 8th International Conference on Computational, pp. 476-485, 2008.

[35] M.C. Lin, L.R. Dung, P.K. Weng, “An ultra-low-power image compressor for capsule endoscope,” BioMedical Engineering Online, 5:14, pp. 1-8, 2006.

[36] C. Cheng, Z. Liu, C. Hu, and M. Meng, “A novel wireless capsule endoscope with JPEG compression engine,” in Proc. of IEEE International Conference on Automation and Logistics, pp. 553-558, 2010.

[37] C. Hu, M. Meng, L. Liu, Y. Pan, and Z. Liu, “Image representation and compression for capsule endoscope robot,” in Proc. of IEEE International Conference on Information and Automation, pp. 506-511, 2009.

[38] J. Wu and Y. Li, “Low-complexity video compression for capsule endoscope based on compressed sensing theory,” in Proc. International Conference of the IEEE Engineering in Medicine and Biology Society, pp. 3727-3730, 2009.

[39] L. Dung, Y, Wu, H. C. Lai, and P. Weng, “A modified H.264 intra-frame video encoder for capsule endoscope,” in Proc. of IEEE Biomedical Circuits and Systems Conference, pp. 61 – 64, 2008.

[40] T. H. Khan and K. Wahid, “Low power and low complexity compressor for video capsule endoscopy,” IEEE Transactions on Circuits and Systems for Video Technology, vol. 21, no. 10, pp. 1534-1546, 2011.

[41] Tareq H. Khan and Khan A. Wahid, “Universal Bridge Interface for DVP-compatible Image Sensors,” Microprocessors and Microsystems, Elsevier, vol. 35, pp. 547-556, 2011.

[42] M. C. Lin and L. R. Dung, “A Subsample-Based Low-Power Image Compressor for Capsule Gastrointestinal Endoscopy,” EURASIP Journal on Advances in Signal Processing, vol. 2011, 257095.

[43] J. Thone and et. al. “Design of a 2 Mbps FSK near-field transmitter for wireless capsule endoscopy,” Sensors and Actuators A: Physical, vol. 156, no. 1, pp. 43–48, 2009.

[44] Amjed S. Al-Fahoum and Ali M. Reza,"Perceptually Tuned JPEG Coder for Echocardiac Image Compression,” IEEE Transaction on Information Technology in Biomedicine, vol. 8, no. 3, 2004.

[45] S. Wu and A. Gersho, "Rate-constrained picture-adaptive quantization for JPEG baseline coders," in Proc. of IEEE International Conference on Acoustics, Speech, and Signal Processing, pp.389-392, 1993.

[46] K. Ramachandran and M. Vertterli, "Rate-distortion optimal fast thresholding with complete JPEG/MPEG Decoder compatibility," IEEE transaction on image processing, vol. 3, no. 5, 1994.

[47] Lan-Rong Dung and Yin-Yi Wu, "A Wireless Narrowband Imaging Chip for Capsule Endoscope," IEEE Transactions on Biomedical Circuits and Systems, vol. 4, Issue: 6, pp. 462 – 468, 2010.

[48] T. H. Khan and K. Wahid, "Lossless and low power image compressor for wireless capsule endoscopy," VLSI Design, Hindawi Publishing Corporation, vol. 2011, 2011.

[49] Z. Liao, C. Xu and Z.-S. Li, "Completion rate and diagnostic yield of small-bowel capsule endoscopy: 1 vs. 2 frames per second," Endoscopy, vol. 42, pp. 360–364, 2010.